NON-CONTACT BREATHING ABNORMALITY DETECTION USING MACHINE LEARNING

by

Sefa Erdoğan

B.S., in Mechatronics Engineering, Yıldız Technical University, 2014

Submitted to the Institute of Biomedical Engineering
in partial fulfillment of the requirements
for the degree of
Master of Science
in
Biomedical Engineering

Boğaziçi University
2019

NON-CONTACT BREATHING ABNORMALITY DETECTION USING MACHINE LEARNING

APPROVED BY:

Assoc. Prof. Dr. Ahmet Öncü (Thesis Advisor)	.....
Prof. Dr. Cengizhan Öztürk (Thesis Co-advisor)	.....
Prof. Dr. Ahmet Ademoğlu	.....
Assoc. Prof. Dr. Esin Öztürk Işık	.....
Assist. Prof. Dr. Ömer Ceylan	.....

DATE OF APPROVAL: August 22, 2019

ACKNOWLEDGMENTS

I would like to dedicate my thesis to my family for their love and support. I would like to thank specifically to my nephew Ömer Kerem Erdoğan for adding happiness and joy to my life, motivating me to complete my studies.

I would like to deeply thank my thesis advisors Assoc. Prof. Dr. Ahmet Öncü and Prof. Dr. Cengizhan Öztürk for their guidance and sustained support in all stages of my studies. Working in Assoc. Prof. Öncü's research group helped me improve myself exceedingly.

I would like to thank my friends Berk Omuz, Fikriye Öz, Şener Yilmaz and Meryem Şahin for the productive discussions about both the hardware and the software parts of this thesis.

I would like to thank Miltek R&D company for letting me use their measurement systems.

I would like to thank my subjects work their patient and cooperativeness during the breathing measurements.

ACADEMIC ETHICS AND INTEGRITY STATEMENT

I, Sefa Erdoğan, hereby certify that I am aware of the Academic Ethics and Integrity Policy issued by the Council of Higher Education (YÖK) and I fully acknowledge all the consequences due to its violation by plagiarism or any other way.

Name :

Signature:

Date:

ABSTRACT

NON-CONTACT BREATHING ABNORMALITY DETECTION USING MACHINE LEARNING

Respiratory diseases are widely seen in the world and they are not seriously handled until they start affecting the patient's life very badly. Respiration motion contains information about the patient's health status which can be measured with non-contact measurement techniques. Non-contact continuous measurement of respiration rate and pattern is desirable for both the patients and the caregivers. Doppler radar can measure the chest wall displacement, accurately. It is also cheap and accessible. Once the chest wall motion is captured, machine learning algorithms can predict the type of the breathing pattern. Different types of breathing patterns contain distinctive features that the classification algorithms can focus on. In this study, a Doppler radar measurement setup was prepared. The accuracy of the system was tested with a linear actuator and it found to be accurate enough to measure the chest wall displacement. 5 breathing patterns including normal, hypoventilation, Kussmaul, Cheyne-Stokes and Biot's breathing were collected from 10 subjects. Since each subject reproduced 5 breathing patterns, a total of 50 measurements were taken. Results show that prediction accuracy is 96% for linear discriminant and subspace ensemble classifier, and other used algorithms also predict the patterns with more than 90% accuracy.

Keywords: Doppler radar, Non-contact measurement, Classification, Breathing disorder.

ÖZET

MAKİNE ÖĞRENMESİ İLE TEMASSIZ NEFES BOZUKLUĞU ÖLÇÜMÜ

Solunum hastalıkları dünyada sıklıkla görülmektedir ancak hastanın hayatı çok ciddi şekilde etkilenmediği sürece hastalık tedavi edilmemektedir. Temassız ölçüm teknikleriyle ölçülebilen solunum hareketi hastanın sağlık durumuyla ilgili bilgiler içermektedir. Solunum hızı ve hareketinin temassız sürekli ölçümü hem hastalar, hem sağlık çalışanları için istenen bir imkandır. Doppler radar göğüs kafesi hareketini doğru bir şekilde ölçebilir. Doppler radar modül tipi aynı zamanda ucuz ve erişilebilir bir radardır tipidir. Göğüs kafesi hareketi kaydedildikten sonra makine öğrenmesi algoritmaları solunum hareketi tipini tahmin edebilir. Çeşitli solunum hareketlerinin sınıflandırma algoritmalarının odaklanabileceği farklı özellikleri bulunmaktadır. Bu çalışmada, bir Doppler radar ölçüm düzeneği hazırlandı. Sistemin hassasiyeti servo motor konrollü lineer aktüatör ile test edildi ve radarın göğüs kafesi hareketini ölçebilir hassasiyette olduğu tespit edildi. 10 denekten normal, hipoventilasyon, Kussmaul, Cheyne-Stokes ve Biot dahil 5 nefes tipi toplandı. Her denek 5 nefes hareketi ürettiğinden, toplamda 50 ölçüm alındı. Sonuçlar, lineer diskriminant ve alt uzay diskriminant topluluk sınıflandırıcılarının nefes hareketlerini %96 doğrulukla tahmin edebildiğini, kullanılan diğer algoritmaların doğruluklarının ise %90'ın üstünde olduğunu gösterdi.

Anahtar Sözcükler: Doppler radar, Temassız Ölçüm, Sınıflandırma, Nefes bozukluğu.

TABLE OF CONTENTS

LIST OF FIGURES

LIST OF TABLES

LIST OF ABBREVIATIONS

ApEn	Approximate Entropy
BPM	Breath per Minute
C_0	Speed of light
CO_2	Carbon dioxide
CW	Continuous Wave
DT	Decision Tree
DTB	Decision Tree Bagging
ECG	Electrocardiography
f_0	Local oscillator frequency
f_d	Doppler frequency shift
f_t	Radar frequency
FIR	Finite Impulse Response
FMCW	Frequency Modulated Continuous Wave
GHz	Gigahertz
kHz	Kilohertz
kNN	k-Nearest-Neighbor
LDA	Linear Discriminant Analysis
RADAR	Radio Detection and Ranging
RF	Radio Frequency
RIP	Respiratory Indutive Plethysmography
SPI	Serial Peripheral Interface
SVM	Support Vector Machine
v_r	Radial velocity

1. MOTIVATION

Breathing is one of the 5 vital signs, and being able to measure it continuously gives an idea about the person's general health. Any alteration in breathing pattern may be caused by a damaged central nervous system which should be considered by medical professionals.

Radar technologies enable us to detect the speed, direction and the distance of a moving object, remotely. The accuracy of the Doppler radar displacement measurement enables us to detect the chest wall displacement which contains both the heart and respiration motion.

Machine learning algorithms are widely used in many fields including the biomedical technologies. These algorithms are able to classify the time domain signals which makes them useful for breathing abnormality detection. To be able to accurately classify the respiration disorders, good feature selection is an important task.

In this thesis work, a Doppler radar system was used to acquire chest wall displacement. Raw data were analog and digitally processed to extract the displacement information and then features that were thought to represent the respiratory motion signals well were extracted. The best features representing the breathing patterns were selected and fed into the classification algorithms. Linear discriminant analysis was able to classify the breathing patterns with 96% accuracy.

Keywords: Breathing disorder, Biot's, Cheyne-Stokes, non-contact measurement, Doppler, classification, feature extraction, feature selection.

2. INTRODUCTION

2.1 Respiratory patterns

The adequate supply of oxygen is crucial for the functioning of the human body including neurological functions. Lack off oxygen affects the brain functions within seconds, and neurons begin to die within minutes. Respiratory system supplies the requisite gasses from the environment to the body and helps the body's acid-base balance. The driving force of the gas exchange is the pressure difference among inside of the lungs and the environment, and while the diffusion is used to transport the gases over short distances, convection is used for longer distances.

Ventilation is the gas exchange between alveoli and atmosphere, which takes place in the lungs. To create a pressure difference which enables the ventilation, chest and diaphragm works collaboratively. Contraction of inspiratory muscles increases the lung volume, which decreases the inner pressure of the lung lower than that of the environment. This pressure difference is actively generated, and it enables air to rush inside the lungs resulting in the expansion of the thorax. Relaxation of contracted muscles cause the diaphragm to rise, and the lung and chest volumes to decrease.

Ventilation is maintained by the interplay of the central nervous system, lung receptors, and central and peripheral chemoreceptors. Respiratory rhythm is generated by network of neurons that are located at the ventrolateral medulla and controlled by vagus and glossopharyngeal nerves. Chemoreceptor afferents and neurons in the parabrachial nucleus can increase the respiratory rate and depth. Serotoninergic neurons located in the ventral medulla can also affect respiratory rhythm by serving as chemoreceptors. Apnea is a necessary process during the swallow and noxious chemical irritation of airway and, it is produced by neurons in the intertrigeminal zone [1]. Forebrain can alter the respiratory rhythm. Deterioration of any system that affects respiration shows itself in respiration rate, volume, regularity, depth or in motion

pattern [2, 3].

Several metabolic conditions may alter the breathing rate or pattern which is accepted as the first sign of physiological deterioration [4]. Chronic respiratory diseases are frequently seen in all around the world. The most common chronic respiratory diseases are asthma, chronic obstructive pulmonary disease, acute respiratory infections, lung cancer and tuberculosis. Around 235 millions of people suffer from asthma and 200 million suffer from the chronic obstructive pulmonary disease [5]. Being able to detect breathing abnormalities help with the diagnosis and monitoring of the related diseases. Early detection of deterioration can decrease the recovery time and cost, drastically.

2.1.1 Normal Breathing

Respiration is carried out by lungs which is also responsible for buffering the blood volume and filtering the small blot clots from the venous circulation. During the inspiration the diaphragm, scalene muscles and external intercostal muscles contract. This contraction results in the diaphragm to lower and this motion raises and expands the chest which also results in expanded lungs. Conversely, expiration lowers and reduces the chest and the lung volume. In [2], this cyclic thorax displacement depending on the different subjects is measured in between 4-12 millimeters. For a healthy adult, respiration rate is in between 12-20 breaths per minute (BPM) [4]. Figure 2.1 shows chest wall motion for the normal breathing.

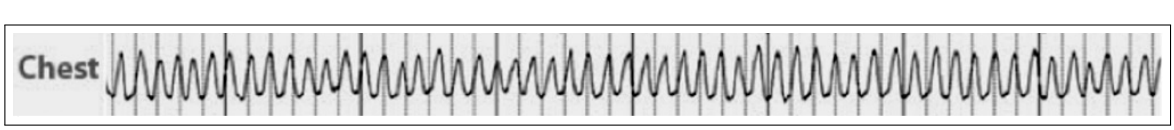

Figure 2.1 Normal breathing pattern. Each large box represents 30 seconds. Adapted from [6].

2.1.2 Kussmaul Breathing

Dr. Adolf Kussmaul observed diabetic patients who were in the late stage of ketoacidosis. He described a new breathing pattern that is deep and rapid and is caused by severe metabolic acidosis. Kussmaul breathing is more commonly seen in diabetic ketoacidosis, lactic acidosis, sepsis and less common in salicylate poisoning, renal tubule acidosis and diarrhea [7]. Figure 2.2 illustrates Kussmaul breathing pattern.

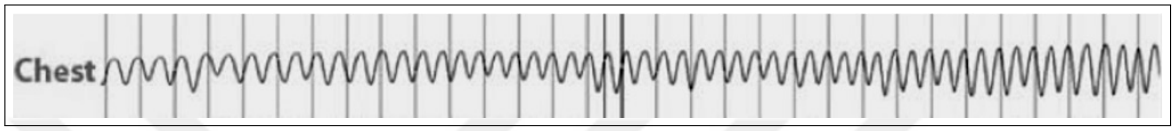

Figure 2.2 Kussmaul breathing pattern. Each large box represents 30 seconds. Adapted from [6].

2.1.3 Hypoventilation

Hypoventilation is a condition of decreased depth and respiratory movement. Patients with this condition exhale less CO_2 than the rate of CO_2 they produce. It causes unbalanced partial pressure of CO_2 level. Chest injury, neuromuscular disorders, Batter's syndrome and adrenal steroid excess are some of the causes of hypoventilation [1].

2.1.4 Cheyne-Stokes Breathing

Cheyne-Stokes breathing is described as cyclical, increasing-decreasing breathing pattern followed by apnea. This type of breathing is generated by normal brainstem respiratory reflexes [8, 9]. For a healthy person, there are only a few seconds of circulatory delay between a change in alveolar blood gasses and CO2 tension in the brain. Although cardiovascular or pulmonary diseases increase the circulatory delay, descending pathways sustain the breathing even during no need for respiration. This feature damps the oscillation that causes Cheyne-Stokes. Bilateral damage, hepatic failure,

uremia and heart failure that prolongs blood reach from lungs to brain [1].

Cheyne-Stokes is commonly seen in patients who suffer from brain tumor, traumatic brain injury, carbon monoxide poisoning and stroke. It is also mentioned in the literature that among the patients who had heart failure, those who have Cheyne-Stokes breathing pattern have a worse course of disease than those who do not have it [7]. Figure 2.3 illustrates the Cheyne-Stokes breathing pattern.

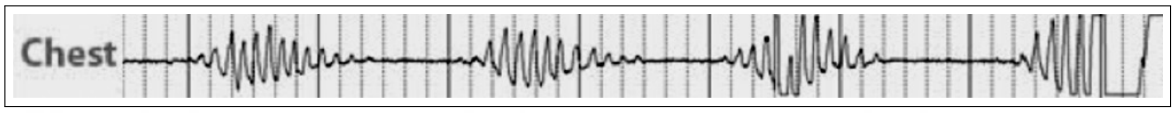

Figure 2.3 Cheyne-Stokes breathing pattern. Each large box represents 30 seconds. Adapted from [6].

2.1.5 Biot's Breathing

In the 19th century, Camille Biot studied patients who had Cheyne-Stokes breathing and in one patient he observed that rather than regular gradually increased and decreased respiratory movements, patient had irregular crescendo and decrescendo cycles following apnea segments were seen for both Cheyne-Stokes and Biot's breathing patterns. So, Biot concluded that this breathing pattern should be named different than Cheyne-stokes. This type of breathing abnormality is seen in patients with brain stem injury, medullary lesions, narcotic medications and chronic opioid abuse [7, 10]. Figure 2.4 illustrates the Biot's breathing pattern.

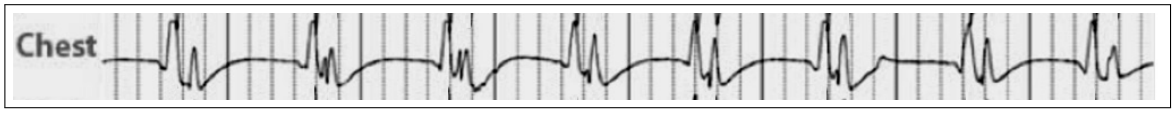

Figure 2.4 Biot's breathing pattern. Each large box represents 30 seconds. Adapted from [6].

2.2 Vital Sign Measurement Techniques

2.2.1 Contact-based Measurements

There are several methods being used by contact-based respiration monitoring. Respiration measurement devices can be acoustic based, airflow based, rib cage and abdominal displacement detection based, transcutaneous CO_2 monitoring based or electrocardiogram (ECG) derived respiration rate based. In [11], Mimoz et al. were able to accurately measure the respiration rate with an acoustic transducer. The results of acoustic transducer were tested by comparing its results to an airflow measurement based capnometer. To assess the accuracy of the respiration rate statistically, Bland-Altman analysis method was performed.

Respiratory inductive plethysmography (RIP) is another contact-based respiratory monitoring device that measures the rib cage and abdomen circumference. Zhang et al. in [12] present a RIP module with accurate lung volume estimation and low power consumption.

ECG derived respiration rate measurement technique uses the modulation effect of respiration over the ECG signals. Respiration rate can be extracted from ECG signals by measuring the respiratory induced fluctuations. Mazzati et al. [13] monitors respiratory waveform, frequency and apnea and results were compared with the nasal/oral flow.

Oximetry probe-based devices emit and collect red and infrared frequencies to measure the blood oxygen saturation. The oxygenated hemoglobin absorbs more infrared frequencies and less red light frequencies, and the oxygenated hemoglobin absorbs more red light and less infrared light [14].

Fekr et. al developed a contact-based respiratory abnormality detection system using an accelerometer sensor [15]. They have used hierarchical Support Vector Machine (SVM) algorithm to detect five types of breathing abnormalities. The average

accuracy of the system found to be 82.29% for 11 subjects. In [16], Fekr et. al conducted another investigation on breathing abnormality detection with 10 subjects and eight types of breathing abnormalities, using six different classification algorithms. The best accuracy was found to be 97.50% in SVM and second best algorithm for the study group was found to be 97.37% with decision tree bagging (DTB). The measurements were again taken with contact-based accelerometer.

2.2.2 Non-contact Measurements

Non-contact vital sign detection is widely studied in the literature [17–22]. In [17], Lohman et al. studied Doppler radar vital sensing and the low-pass filtered the respiration signals with 0.7 Hz cut-off frequency to extract the respiration motion and band-pass filtered the unfiltered signal with 1-3 Hz cut-off frequencies to extract heart rate. They used autocorrelation method to estimate the heart rate and respiration rate and concluded that 88% of the time their estimations were correct compared to reference rate taken from pressure pulse sensor UFI-1010. Suzuki et al in their work [19] used dual-frequency microwave radars to monitor vital signs for elderly care. They located their two 24 GHz radars underneath the mattress to measure the heart rate and respiration rate. An electrocardiogram was used as a reference measurement system and their system was r=0.92 correlated for the heart rate measurement. Also they found the respiration rate correlation coefficient as 0.94.

Lee et al. [22] suggest to decompose the inhalation and exhalation segments for more detailed information investigation. They also suggest continuous wavelet transform for detailed analysis of the respiratory patterns. They found strong correlation between Doppler radar and spirometer during tidal volume estimation. Rahman et al. [23] were able to accurately predict which subject is breathing behind the wall by just looking at their similar breathing patterns. They proposed to zoom in the segments of the breathing cycle and also increase the signal to noise ratio by manipulating the DC offset. They used 2 subjects 14 breathing patterns and all the predictions were correct. Miao et al. [20] used Doppler radar for monitoring the 4 different breath-

ing patterns including normal, Cheyne-Stokes, dysrhythmic and Kussmaul's breathing types. Then by using support vector machine (SVM) classifier and six different kernel functions, they found that the best accuracy for the classification of the breathing patterns was 93.3%. They have used 5 different subjects and 60 samples were taken from these subjects. The linear SVM was predicted correctly all the normal and Cheynes-Stokes instances. While the dysrhythmic breathing was predicted with 80% accuracy, Kussmaul's breathing was predicted with 93% accuracy. Another Doppler radar based system is [21] which detects sleep quality by measuring the heart rate, respiration rate and body motion. They collected 110 hours of sleep data from 8 subjects and they used an ARM microcontroller and an Android smartphone to handle machine learning algorithms. The heart rate error of the device was found 8.07% and respiration rate error was found 10.84%. ffff

2.3 Radar Principles

A Radio Detection and Ranging (RADAR) device generates radiating electromagnetic energy and receives the returning echo signals that are reflected from the objects. The distance of the object from the radar can be extracted from the travel time. Travel time is the sum of the transmitted signal's duration to hit the object and reflected signal's duration to the hit the radar receiver. If the target is stationary, then the phase and frequency of the reflected signal do not change. However, if the target is moving, received signal's (reflected signal) phase is shifted and therefore the velocity of the target's movement can be found by signal processing. Depending on the size, material and geometry of the target, the received signal's power changes. By choosing the appropriate frequency, radar signals can penetrate through walls, clouds, dust or blankets which enables to detect invisible targets. The frequency range for radar is usually defined as 3 kHz to 300 GHz, and both resolution and atmospheric attenuation increases with higher frequencies for pulsed radar systems [2, 24, 25].

Figure 2.5 car curt shows the typical radar system components. A radar system has a transmitter, a receiver, an antenna and a signal processing unit. The transmit-

ter is responsible for generating the electromagnetic waves and amplification of it to the required power. An antenna concentrate the radio waves to the desired direction and receive the echo signals from the same direction. Using this property, the target's direction can be detected. The receiver detects the reflected waves from the objects whose dielectric constants are different and at the direction of the transmitted waves. Then the receiver down converts the received transmission frequency to the intermediate frequency or base-band. It also amplifies the signal for digitization or display purposes, and separates the noise and interference from the signal.

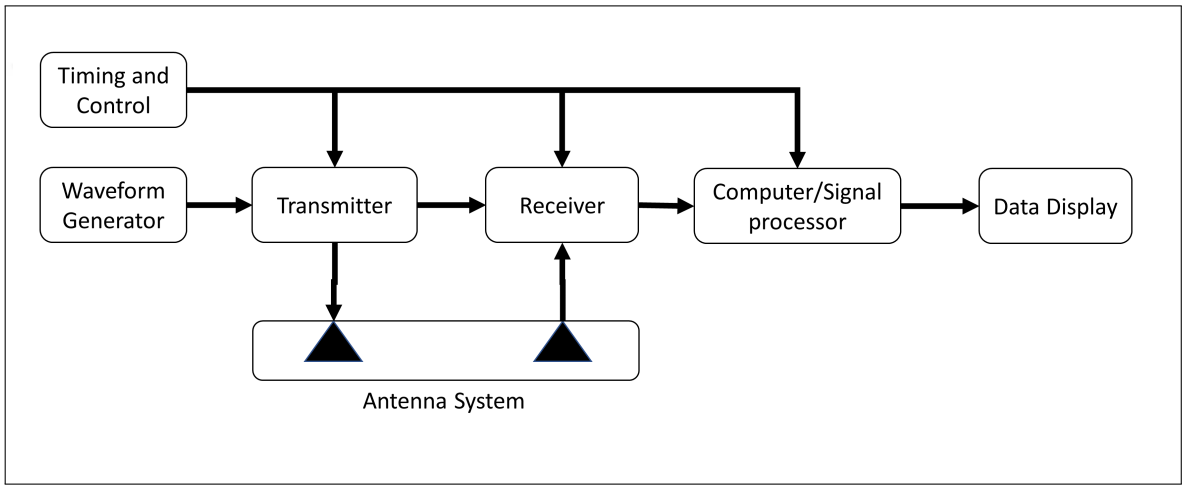

Figure 2.5 Simplified radar block diagram. Adapted from [26].

2.3.1 Doppler Radar

In 1842, Austrian physicist Christian Doppler discovered that the frequency of the reflected waves is shifted if there is a relative movement between object and signal source. Basically, if the relative speed is zero then the radar system reaches the same cycles as the signal source transmits. If the object is getting closer to the radar than the radar reaches more cycles than in stationary state. The reflected Doppler shift is positive if the relative distance increases between the signal source and the object and vice versa. The relation between velocity and the Doppler shift can be expressed with

$$f_d = \frac{2 f_t \nu_r}{C_0} \tag{2.1}$$

where f_d is the Doppler frequency shift, f_t is the radar frequency, ν_r is the radial velocity (m/s) which equals to $v\cos\theta$, and C_0 is the speed of light [27].

Doppler radar systems are widely used in various fields such as vehicle speed measurement, weather forecasting, door opening systems and physiological vital sign detection systems [2, 17, 25]. Several waveforms such as CW, frequency modulated continuous wave (FMCW) and pulsed can be selected depending on the specific requirements of the application.

If we neglect the phase noise and simplify the CW transmitted signal then it can be expressed as:

$$T(t) = \cos(2\pi f_0 t) \tag{2.2}$$

where f_0 local oscillator frequency, t is elapsed time. Transmitted signal travels until it is reflected from an object or human body. If the transmitted signals is reflected from the subjects rib cage which has a relative movement to the transmitter, then the phase shifted received signals can be expressed as:

$$R(t) = A\cos(2\pi f_0 t + \frac{2\pi}{\lambda}(2d_0 + 2d(t))) \tag{2.3}$$

where d_0 is the initial distance between rib cage and radar antenna, and $d(t)$ is the displacement resulting from the breathing and heart beat, and A is the received signal's amplitude.

A simple Radio Frequency (RF) front end contains transmitter, receiver, local oscillator, splitter and frequency mixer. It basically multiplies the transmitted and received signals which results:

$$R(t)T(t) = A\cos(2\pi f_0 t + \frac{2\pi}{\lambda}(2d_0 + 2d(t)))\cos(2\pi f_0 t) \tag{2.4}$$

and from trigonometry,

$$\cos a\cos b = \frac{\cos(a-b) + \cos(a+b)}{2} \tag{2.5}$$

Resulting signal can be expressed as

$$R(t)T(t) = \frac{A}{2}\cos\left(\frac{2\pi}{\lambda}(2d_0 + 2d(t))\right) + \frac{A}{2}\cos\left(2\pi f_0 t + \frac{2\pi}{\lambda}(2d_0 + 2d(t))\right) \quad (2.6)$$

A low pass filter can be used to eliminate the high frequency component of the equation and received baseband signal becomes,

$$R(t)T(t) = \frac{A}{2}\cos\left(\frac{2\pi}{\lambda}(2d_0 + 2d(t))\right) \quad (2.7)$$

and its variable phase can be expressed as,

$$\theta(t) = \frac{2\pi}{\lambda}2d(t) \quad (2.8)$$

Simply by taking the arccos of the sensor output, chest wall displacement can be found [2]. This type of radar is called single channel radar system, and its main disadvantage is the null point limitation which was described in [28] as loss of sensitivity at distances;

$$d_0 = \frac{n}{4}\lambda \quad (2.9)$$

if the n is an integer. Figure 2.6 illustrates the single channel Doppler radar system.

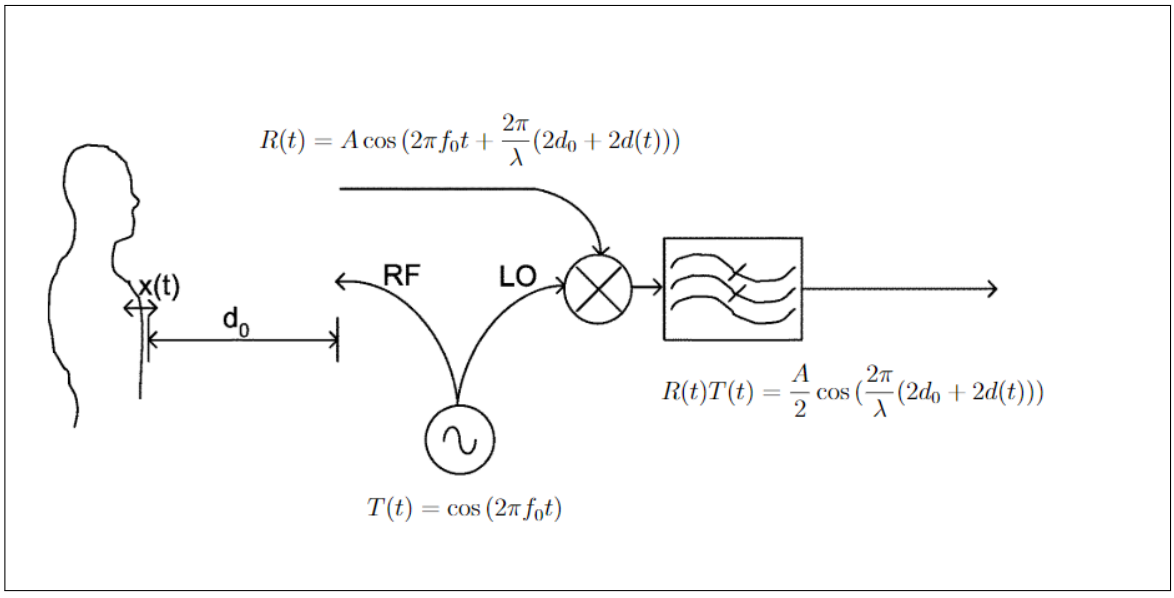

Figure 2.6 Single channel Dopper radar illustration. Adapted from [29].

Quadrature receiver system is proposed by [29] to overcome the null point limitation problem. In quadrature systems there are two output ports which are called in-phase and quadrature channels. Quadrature channel output is generated by phase shifting the local oscillator signal by 90° and then mixing it with the received signal. So, while the quadrature channel term contains sine function, in-phase channel contains cosine function. By taking the arctangent of two output channels,

$$\phi(t) = \arctan\left(\frac{Q(t)}{I(t)}\right) = \arctan\left(\frac{\sin\left(\theta + d(t)\right)}{\cos\left(\theta + d(t)\right)}\right) = \theta + d(t) \tag{2.10}$$

where $d(t)$ is the superposition of respiratory and heart motion can be found. So, the respiration motion's phase information $x(t)$ and the heart motion's phase information $y(t)$ can be expressed as $d(t) = 4\pi(x(t)+y(t))/\lambda$. If the measured displacement is bigger than the half wavelength of the carrier signal, unwrapping is needed. Thereafter, the equation

$$\Delta X = \frac{1000C_0}{4\pi f}\arctan\left(\frac{Q(t)}{I(t)}\right) \tag{2.11}$$

can be used to find the chest wall displacement (ΔX) in millimeters where f is the Doppler radar's carrier frequency [30].

A more comprehensive equation which includes quadrature channel imbalance, DC offset and phase error can be written as

$$\phi'(t) = \arctan\left(\frac{Q(t)}{I(t)}\right) = \arctan\left(\frac{V_Q + A_e\sin\left(\theta + d(t) + \phi_e\right)}{V_I + \cos\left(\theta + d(t)\right)}\right) \tag{2.12}$$

where V_I and V_Q are the DC offset and A_e and ϕ'_e are the amplitude error and phase error, respectively [2, 31].

2.4 Machine Learning Approach

Predicting the possible future actions of a system or extracting the hidden information in a respiration motion can be accomplished by programming computers. Given a set of data from the chest wall motion of several patients and healthy subjects, ma-

chine learning algorithms select some parameters and optimize the selected parameters in the training phase. Selected parameters are expected to express the original data well. Systems where the features and their labels are clearly given to the algorithm are called supervised learning. Since the algorithm has access to the structure of the data, new data can be classified according to the specific properties of the algorithm. In this section, extracted features and applied classification algorithms will be described.

2.4.1 Feature Extraction and Selection

Finding the most expressive features for each class is one of the most important tasks for machine learning algorithms. By choosing the most relevant k dimensions (features) that can carry most of the information of the original data, classification speed increases and the complexity of the algorithm decreases. Furthermore, although mostly increasing the number of features results in better training error, it does not necessarily lower the validation error which is loss of the time and effort [32]. Several features described below was used in this thesis to help classify the different breathing patterns.

Number of peaks: In a selected time window, the number of peaks represents how many breath is taken. Peak is found at the location where the inhalation ends and exhalation starts.

Peak average: From a selected time window, amplitudes of peaks were found from the breathing signal and then mean value is calculated from these amplitudes. Peak average represents the average depth of the subject‘s breath.

Maximum amplitude: Maximum value of the breathing pattern signal. It gives the subject‘s deepest breath from a selected time window.

Peak Variance: Variance of a signal is average squared deviation from the mean, and it shows the variability within the signal. In this work, it represents the variance of the tidal volume.

Maximum Value of the Short-time Signal: Short term energy of 5 seconds sliding

window was first calculated. To calculate the energy of the signal, equation:

$$\sum_{n=0}^{N} |x(n)^2| \tag{2.13}$$

is used. The resulting energy matrix is shorter than original breathing pattern matrix and it has its own maximum, minimum, variance value. Maximum value of the new matrix is selected as short-time maximum value. Before the calculation of the short term energy, the signal was normalized to between 0 and 1 by dividing its each component to the maximum value of the original matrix.

Minimum Value of the Short-time Signal: Minimum value of the short-time energy matrix.

Range of the Short-time Signal: Maximum value of the short-time signal is subtracted from minimum value of the short-time signal to find the range of the short-time signal.

Variance of the Short-time Signal: Variance of the short-time energy matrix.

Maximum Value of the Instant Frequency: First to find the instantaneous frequency, unwrapped instantaneous phase angle divided by 2π and the derivative is taken. Then the maximum value of the new matrix is selected as the maximum value of the instantaneous frequency.

Minimum Value of the Instant Frequency: Minimum value of the instant frequency matrix.

Range of the Instant Frequency: Range of the instant frequency matrix is calculated with subtracting the maximum value of the instantaneous frequency from minimum value of the instantaneous frequency.

Variance of the Instant Frequency: Variance of the instant frequency matrix.

Mean of the Instant Frequency: Mean of the instant frequency matrix.

Approximate Entropy: From a selected time series window, approximate energy (ApEn) measures the randomness and regularity of a signal. ApEn is well explained in [33] and formulated as

$$ApEn(m, r, N) = \phi_m(r) - \phi_{m+1}(r) \tag{2.14}$$

where

$$\phi_m = (n = m + 1) \sum_{i=1}^{N-m+1} \log C_i^m(r) \tag{2.15}$$

and $C_i^m(r)$ is the number of j such that $d[x(i), x(j)] < r/(N - m + 1)$ where

$$d[x(i), x(j)] = max_{k=1,2,...,m}(|u(i + k - 1) - u(j + k - 1)|) \tag{2.16}$$

from a time series of data $u(1), u(2), ..., u(N)$. Typically, m is set to 2 and r varies depending on the application, and it is considered to be in between 0.1-0.2 times the standard deviation of the time series data [34].

Kurtosis: To detect the distribution of the data and depending on the kurtosis result, it tells information about the shape of the distribution. The kurtosis of a signal is

$$\beta_2 = \frac{E(X - \mu)^4}{(E(X - \mu^2))^2} = \frac{\mu_4}{\sigma_4} \tag{2.17}$$

where E is the expectation operator, X is the input signal, μ is mean of the input signal.

Apnea Score: This feature tries to give higher scores to the breathing patterns that contain apnea. The algorithm calculates the standard deviation of the signal first. Then takes the derivative of the signal to set the apnea segment to the zero amplitude. As a final step, a the algorithm finds how many points lay in between $\pm$ 0.2 standard deviation from the mean of the signal.

After the extraction of features, to be able to express the target best, feature selection must be performed. Any feature that is highly correlated with other features will increase the risk of misleading the classification of the data. Multivariate feature selection can be done using filter, wrapper or embedded methods. Filter methods were used in this thesis and they include correlation, variance thresholding and linear discriminant analysis.

2.4.2 k-Nearest Neighbor

k-Nearest-Neighbor (kNN) is a supervised classification algorithm that classifies the new data point with respect to its k closest neighbor. Supervised algorithms need labeled data sets and kNN is no exception. To assign the new object to a classifier, it is wise to choose k value odd-numbered, since it increases the chance of not having equal votes and tie for the new object's assignment. The distance of the new test object to each point can be found with several distance functions. Depending on the effectiveness on the data set, distance function can be Euclidean, Manhattan, Minkowsky, Camberra, Chebychev, Hamming or other less popular distance functions. Euclidean distance is widely used and can be described as;

$$D(x, y) = \sqrt{\sum_{i=1}^{k} |x_i - y_i|^2} \tag{2.18}$$

The algorithm is memory-based and although it does not need a training phase and model creation is easy, it still needs to compute each point's distance information which makes it slow and computationally expensive.

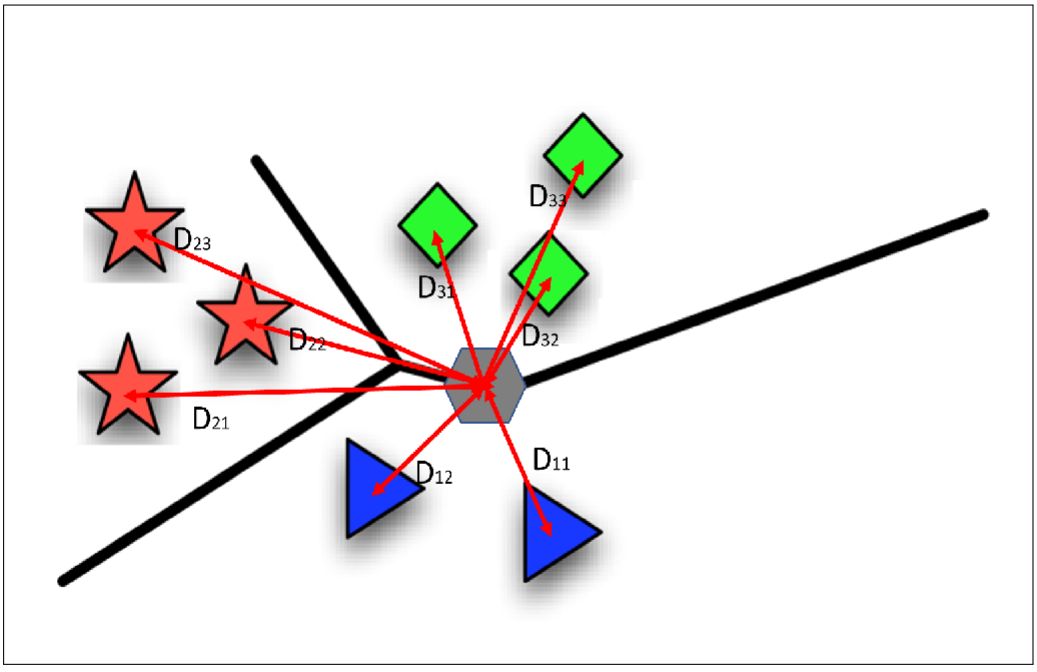

Figure 2.7 Illustration of new grey hexagon data point and its distances to closest neighbors. Adapted from [35].

2.4.3 Decision Tree

Decision tree is a common nonparametric method which is structured as a tree and have root nodes, decision nodes and leaf nodes. Branches are the possible outcomes of the previous node and they determine the direction to the new nodes. Root node has no incoming edge and it is the starting point of the tree. Decision nodes have one incoming edge and have at least two branches. New nodes represent smaller regions which are divided into a smaller nodes until they reach to a leaf node. Leaf nodes or also called end nodes are the class predictions and they only have one incoming edge. Any new data that falls in to this leaf node has the same label if it is a classification problem and similar numeric results for regression problem [32]. Figure 2.8 illustrates a decision tree and its data set which desired to be classified either to C1 or C2.

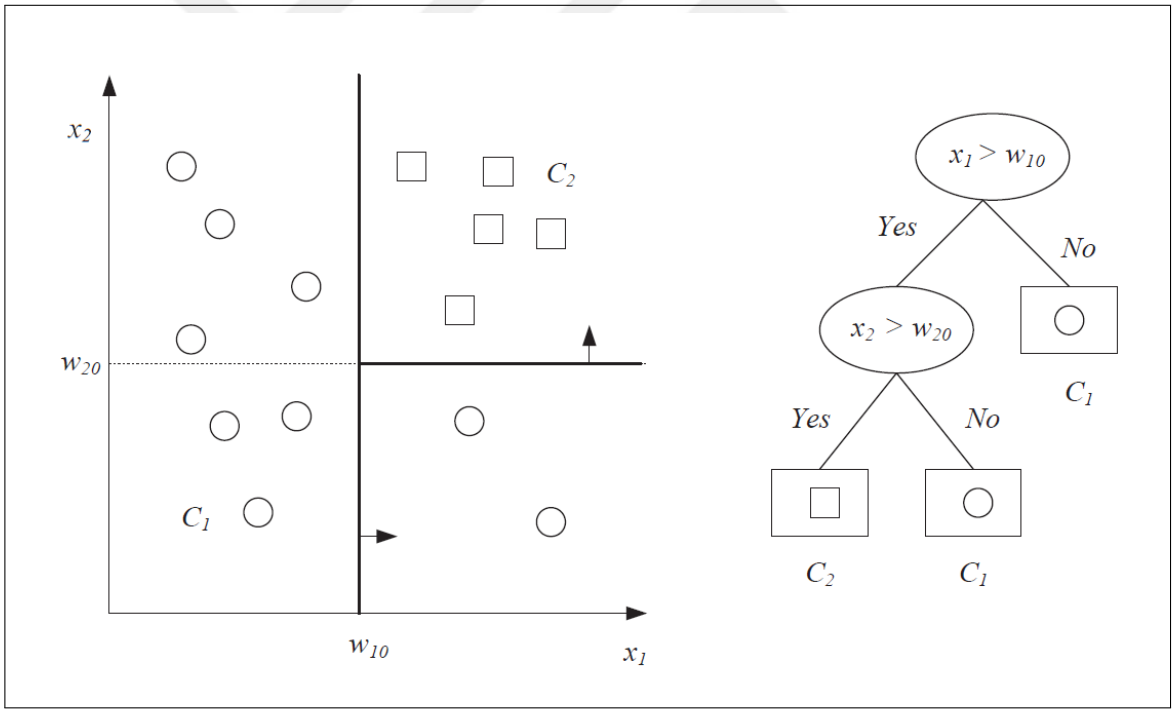

Figure 2.8 Dataset and its decision tree. Adapted from [32].

A commonly used method divide and conquer is developed by Quilan et al. [36] and split the data according to the feature that has the most discriminative subset. The procedure continues until the decision node reaches to the leaf node.

2.4.4 Support Vector Machine

Support vector machine (SVM) is another supervised learning algorithm which can be used for both regression and classification. This classifier tries to maximize the margins of hyperplane so it is robust to outliers. This hyperplane is the place where two data set are the most distinct and support vectors are the closest boundries to the data set. Figure 2.9 shows the optimal hyperplane which is between black dot line and linear separator with black line [32].

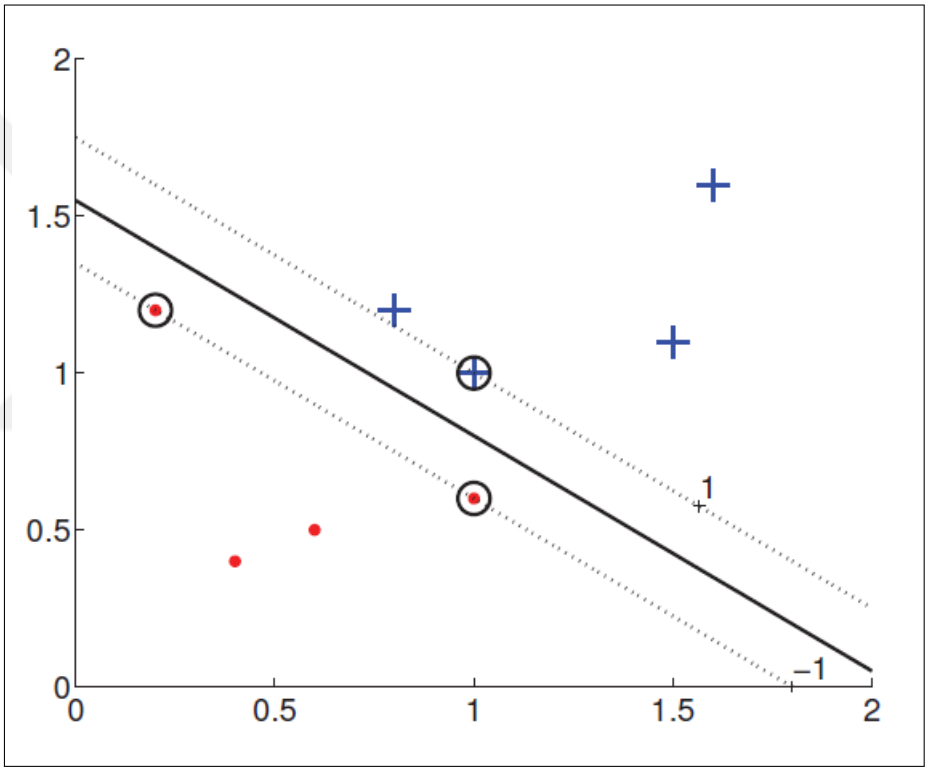

Figure 2.9 Support vector machine illustration. Adapted from [32].

Although the classifier requires high memory and time for the training, by using the kernel functions it is not required to have the nonlinear mapping. This is done by applying a transformation and generates a new feature set. Two kinds of kernel functions are linear kernel and polynomial kernel functions [20].

2.4.5 Linear Discriminant Analysis

Linear discriminant analysis (LDA) is commonly used supervised algorithm for dimension reduction and classification of the data set. It was created by R.A. Fisher in 1936. The algorithm tries to find the best linear transformation that can discriminate among classes. To evaluated the accuracy of the separation, distance between two groups is found by any euclidean distance formula. The result shows how much the classes differ in terms of standard deviations. To classify a new data point, the algorithm checks whether or not the data satisfies below inequality:

$$\beta^T \left(x - \left(\frac{\mu_1 + \mu_2}{2} \right) \right) > -\log \frac{p(c_1)}{p(c_2)} \tag{2.19}$$

where β^T is coefficients vector, x is the data vector and the right side of the inequality is the class probability. The classifier assumes that data can be separated by their distribution functions. It works well even though the data is not normally distributed [37].

2.4.6 Gaussian Naive Bayes'

Gaussian naive Bayes' is a probabilistic classifier algorithm which basis Bayesian theorem and it is called naive because the algorithm ignores the correlations and dependencies. It means any feature that is used for classification purpose excepted to be unrelated to other features. The algorithm uses equation below to find the probability of the event $P(e)$ occur:

$$P(e|Y) = \frac{P(Y|e) * P(e)}{P(Y)} \tag{2.20}$$

where $P(e|Y)$ is the posterior probability of the class for given predictor and e is the class variable and Y is the features, $P(Y|e)$ is the likelihood, $P(e)$ is the prior probability of e and $P(Y)$ denotes the prior probability of the predictor [32, 35].

2.4.7 Subspace Discriminant Ensemble

Subspace Discriminant Ensemble uses the outputs of several classification algorithms including a weak learner and gives the results of the best performing combination. It generally results better than single classification algorithm. This method is more suitable for cases where the number of features is high.

3. METHODS AND EXPERIMENTAL SETUP

3.1 Preliminary Doppler Radar Measurement Setup

To be able to detect heart and respiratory rate in real-time, an ARM-based microcomputer was utilized to Doppler radar measurement system was build. Hardware of the designed system includes an ARM-based microcomputer, power regulators, band-pass filters, amplifiers, analog-to-digital converter, IPS -154 Doppler radar transceiver. Figure 3.1 shows the designed system's block diagram.

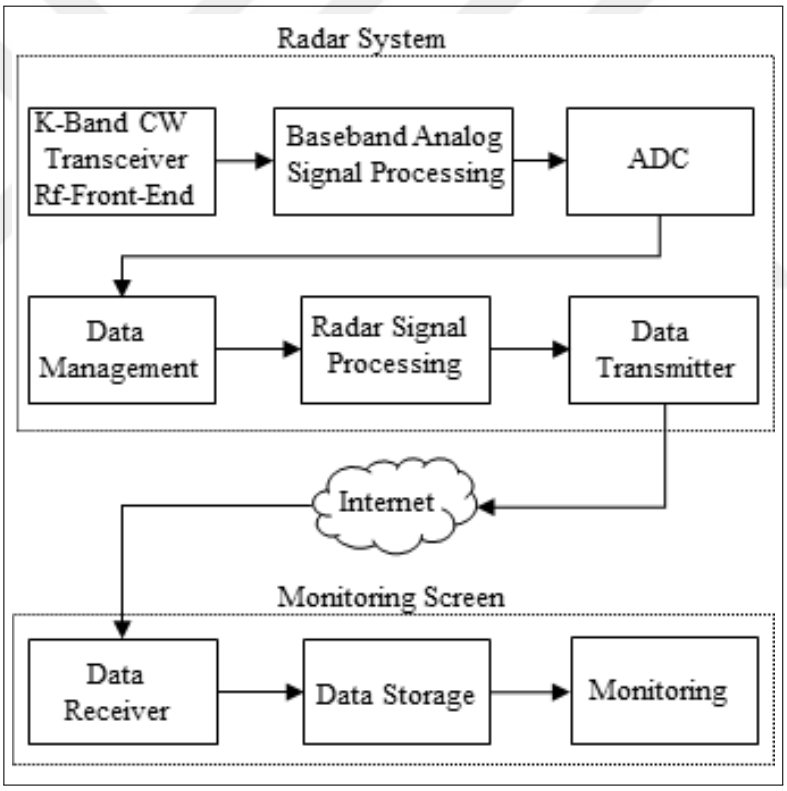

Figure 3.1 Block diagram of the designed Doppler radar measurement system.

IPS -154 is responsible for transmitting and receiving the 24 GHz electromagnetic waves and converting to the base band quadrature signals. Allocated power supply of the RF front-end is low noise RF regulator and ARM-based microcomputer does not use the same power supply. These baseband signals are then fed to ampli-

fiers which have the gain of 20 chosen by empirically for 1 m distance measurements. Amplified signals are then band-pass filtered with 0.0005 Hz lower cut-off and 40 Hz higher cut-off frequency for the DC cancellation and antialiasing purposes. To be able to digitize the data, quadrature signals are then carried with 1.25 volts DC signal. A 12 bit ADC is used to digitize the data which then transmitted to ARM-based microcontroller with serial peripheral interface (SPI) protocol. Sampling rate is set to 160 Hz for minimizing the band interface. The digitized data then signal processed to extract the respiration and heart rate.

The software of the designed Doppler radar measurements system extracts the respiratory rate and the heart rate by following the steps plotted in Figure 3.2.

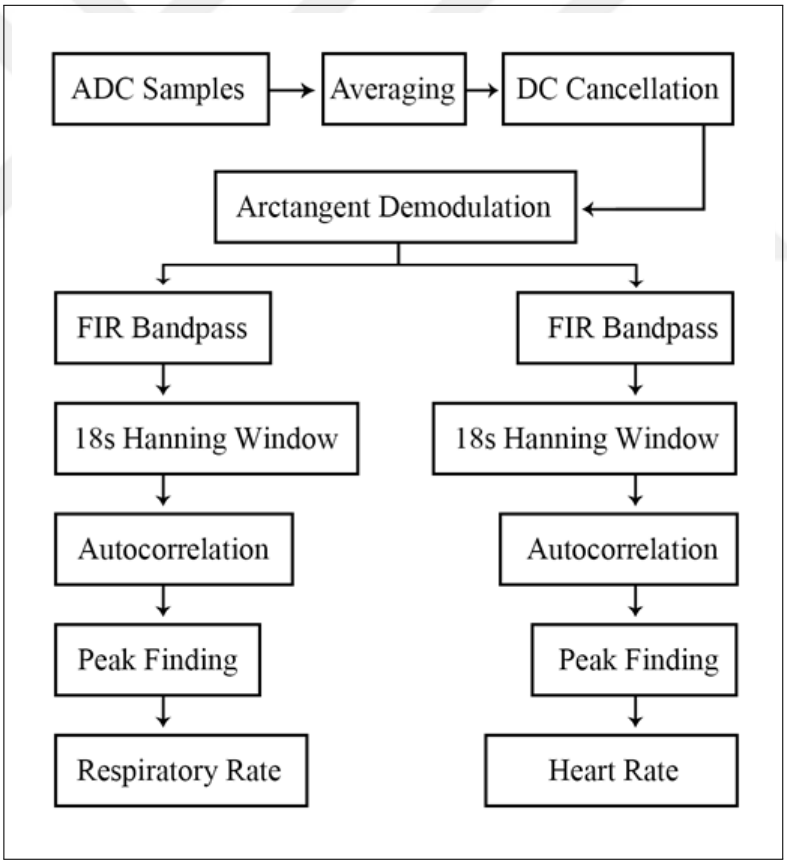

Figure 3.2 Block diagram of the digital signal processing steps of the designed Doppler radar measurement system.

Digitized data first averaged and DC cancelled by using several digital differentiators and integrators. Quadrature signals are then arctangent demodulated and

resulted signals represents the chest wall motion in wrapped radians. Before converting the data to distance, unwrapping is done and radians are converted to angle. Distance conversion of the angle is done by using Eq. 2.11. Respiration rate and heart rate are extracted from the same motion informaition by filtering with 2 different FIR filters. For the respiration rate, cut-off frequency was set to 0.7 low pass filter and for the heart rate cut-off frequencies were set to 1 Hz to 3 Hz band-pass filter. For both respiration and heart rate signals an 18 seconds long Hanning window is applied and resulted signals autocorrelation was calculated. Lastly respiration and heart rate are found by finding the second positive peak of the autocorrelation.

Extracted respiration rate and heart rate are then sent to the internet server with message queuing telemetry transport (MQTT) communication protocol. Since the signal processing is executed on the proposed Doppler radar system and sent to the internet server, any computer that has internet connection can be used to monitor the status of the patient. Displayed physiological data are then stored for further usage. The computer that displays the vital signs is named as subscriber and its graphical user interface was written in Python code. The program has color coded warning for caregivers and it can show multiple subjects status.

3.2 Doppler Radar Setup

Below procedures were followed to be able to transmit and receive the Doppler radar signals, extract displacement information and compare the system's reliability with other distance measurement systems. For each following sections, the Doppler radar distance measurement system containing HMP4030 programmable power supply (Rohde Schwarz, Munich, Germany), LeCroy WaveRunner 6100A 1 GHz oscilloscope (Teledyne LeCroy, New York, USA), K-band transceiver IPS-154 (InnoSent, Geldersheim, Germany) and MATLAB R2019a mathematical computing software (The MathWorks, Inc. Massachusetts, USA) were used as described below.

IPS-154 is a 24 Ghz CW transceiver with 2 channel outputs which are in-phase

and quadrature signals. The transceiver's horizontal full beam width is 45° and its vertical full beam width 38°. It operates with 5V and in this thesis, power is supplied with a LT3042 ultra low-noise RF linear regulator. Linear regulator is supplied with HMP4030 which is also a low noise power supply. Once the IPS-154 is supplied with power, it starts to generate the in-phase and quadrature outputs with respect to the movement in front of it. Generated quadrature signals are then low pass filtered with a 160 KΩ resistor and 0.1μ capacitor which results in 10 Hz cutoff frequency. Filtered channels are then sampled with 500 Hz rate using LeCroy WaveRunner 6100A oscilloscope. Samplings were done with DC 1MΩ coupling, 3 bits noise filtering and 1 sweep pre-processing averaging settings in the oscilloscope. To have synchronous sampling, channel 2 and channel 3 were used. Sampled quadrature channels are then saved to an external hard disk in the MATLAB compatible .mat file format. LeCroy oscilloscope generates 2 .mat output files for one for in-phase and other for quadrature channel. Generated files contain the time variables in their first column, while the second column is the voltage information.

3.2.1 Doppler Radar Signal Processing

To extract the distance information from the digitized quadrature signals, several steps of operations were performed which are shown in Figure 3.3.

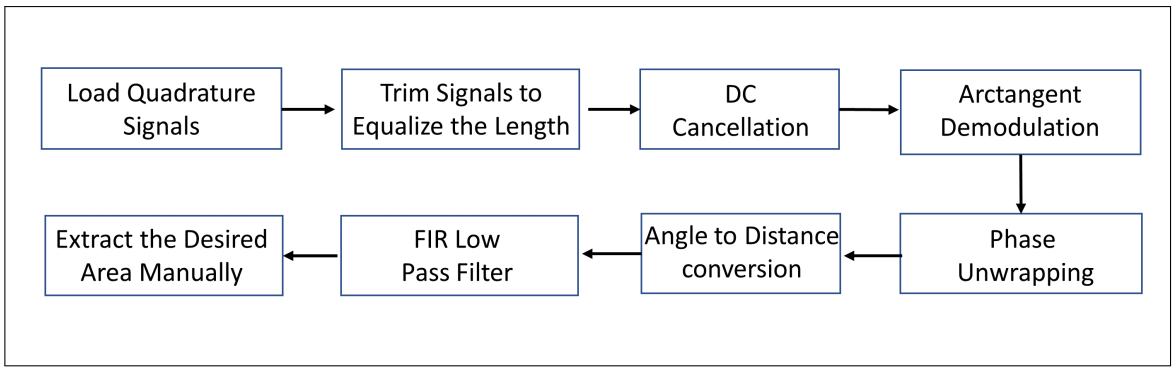

Figure 3.3 Flow chart of the digital signal processing steps for breathing pattern extraction.

Digital signal processing and other codes to compare results, extract features and classification of signals were written in MATLAB R2019a. First, data were imported by a script written and then imported data were trimmed to equalize the length of the data files. DC cancellation was applied by subtracting each channel's mean voltage from itself. Arctangent demodulation was then applied to the quadrature signals using Eq. 2.10. Demodulated signals were in wrapped radian results which needed to be unwrapped to find the distance information. Unwrapping was simply done by adding multiples of $\pm 2\pi$ to the angular data if there is a jump more than π radian between two data points. To convert the angle data to distance, Eq. 2.11 was used. Extracted distance information contains both the respiratory and the heart motion which is later extracted with a Kaiser window finite impulse response (FIR) low pass filter. Cutoff frequency of the filter was selected as 0.7 Hz which caused the filter order to be 6272. Resulted signals contained different breathing patterns and they were manually trimmed to get separate breathing patterns.

3.3 Test Setup with Linear Actuator

To evaluate the accuracy of the designed Doppler radar system, the system was placed 1 meter in front of the linear actuator as it is shown in Figure 3.4. A metal sheet was attached to the linear actuator to reflect the transmitted signals. Linear actuator system was controlled by a program that was written in C# programming language. Position information and elapsed time variables were saved to a text file. To minimize the vibration of the linear actuator system, the speed of the system was set to 5 mm/s and it was programmed to make a 10 mm cyclic periodic movements. To attenuate the servo motor's electrical noise on Doppler radar measurement setup, both systems plugged in different power sources.

Doppler radar measurement setup was the same as it was explained in Section 3.2. Since the sampling frequency of the linear actuator is lower compared to the designed Doppler radar system's sampling frequency, measurements from the linear actuator were linearly interpolated for further investigations.

To evaluate the accuracy of the designed Doppler radar system's measurements with linear actuator's servo motor encoder results, a gold standard statistical analysis method Bland-Altman was used.

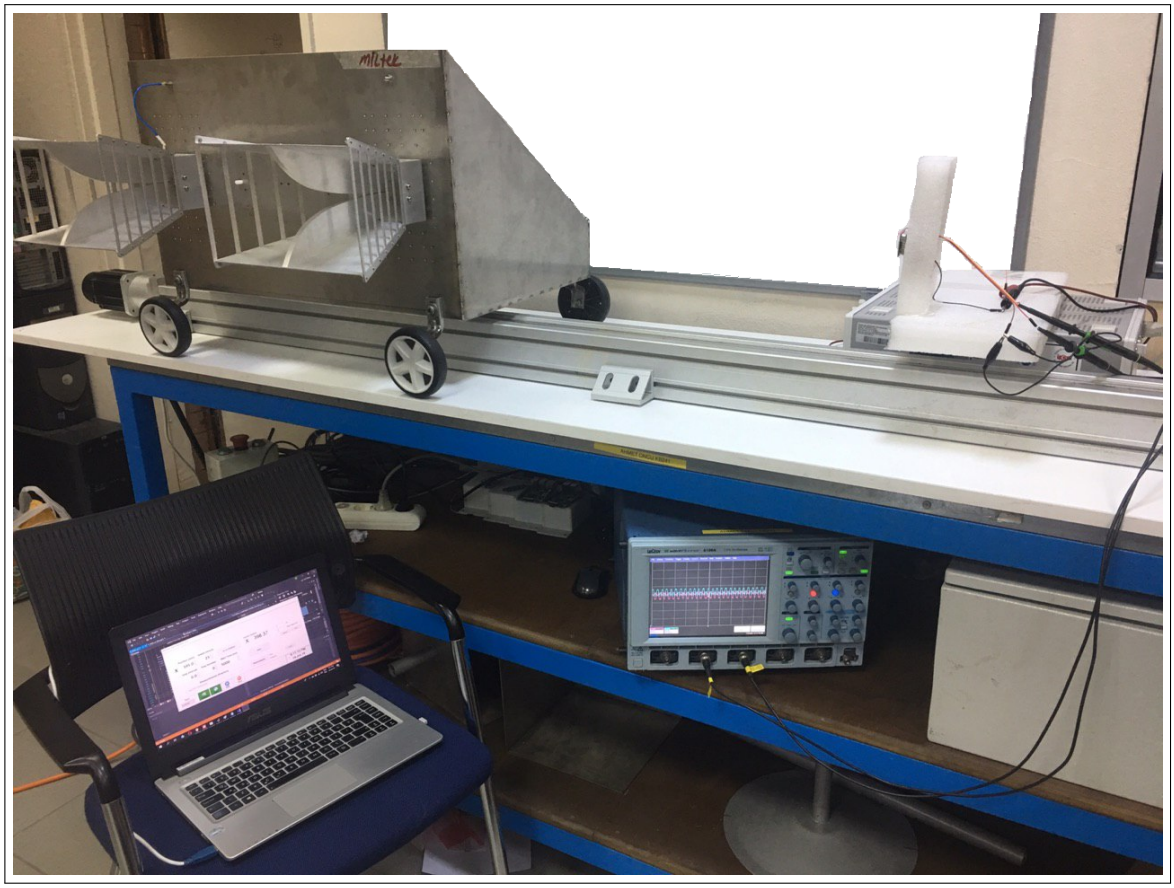

Figure 3.4 Doppler radar test setup with linear actuator.

3.4 Test Setup with Respiratory Belt Transducer and Doppler Radar

Designed Doppler radar system results were also compared with the results from Biopac Respiratory Effort Transducer -MP30 (BIOPAC Systems Inc, CA, USA), while both systems were measuring the same patient's chest wall displacement, simultaneously. Measurements were taken while the subject was wearing respiratory belt transducer on his rib cage and laying on a desk as it is shown in Figure 3.5. Doppler radar

was placed above the patient's rib cage to measure the same area as respiratory belt transducer. It was asked from subject to breathe normally and not to move during the measurements. Respiratory belt transducer measurement results were acquired with Biopac Student Lab Version 3.7.6 software program with 100 Hz sampling rate and saved to a text file. The Doppler radar system's measurement results were collected as it was explained in Section 3.2.

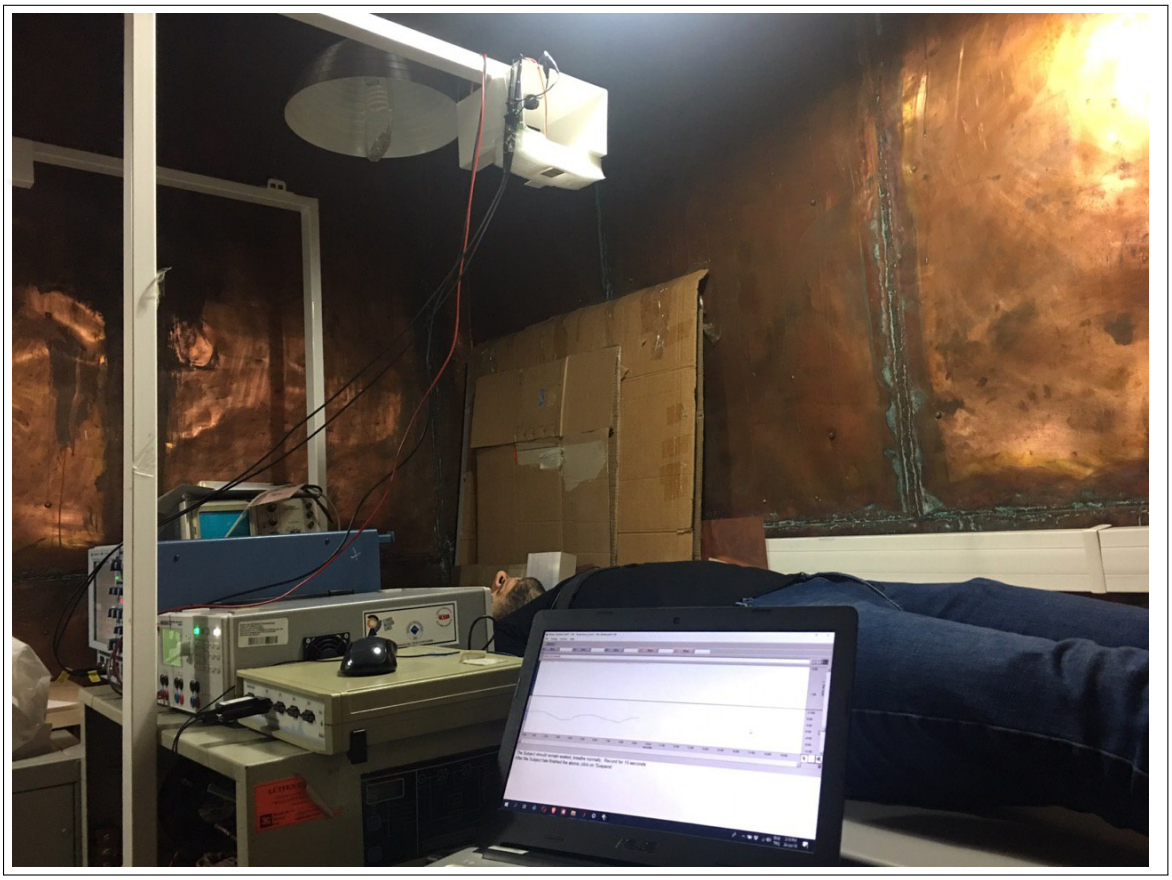

Figure 3.5 Doppler radar test setup with respiratory belt.

3.5 Breathing Measurement Test Setup

To measure 5 different breathing patterns including normal, Kussmaul, Biot's, Cheyne-Stokes breathing and hypoventilation, subjects laid on a desk while the designed Doppler radar system was focused on their chest wall. Subject warned to not to move their body during the test. Subjects were between 19-29 years old who were

students of Boğaziçi University. Breathing patterns were shown to the subjects and they were guided during the measurements as explained below:

Normal Breathing: Subjects were asked to relax and breath normally.

Kussmaul Breathing: Subjects were asked to breath faster and deeper than the normal breathing to increase the frequency and the tidal volume of their respiration.

Biot's Breathing: Subjects were asked to breath faster than the normal breathing with no extra effort to inhale deeper for regular tidal volume. Subject was also asked to hold his/her breath when he/she heard the command "hold" to mimic the periodic apnea of the Biot's breathing.

Cheyne-Stokes Breathing: Cheyne-Stokes breathing pattern was shown to subjects and they were asked to increase the depth of their breath and then, decrease the depth of their breath for the same amount of time as much as possible, and hold his/her breath until the command "Start again".

Hypoventilation: To breathe less than 12 times in a minute, subjects were asked to finish his/her breathing cycle at least 6 seconds or more. Subjects were also asked to breathe less deeply than when they were breathing normally to decrease the tidal volume of their respiration.

Figure 3.6 Breathing measurement test setup.

3.6 Feature Extraction and Selection

Collected breathing pattern signals are first manually trimmed to have 60 seconds of each type of breathing pattern. Since there are 5 breathing patterns to be investigated from 10 subjects, a total of 35 breathing signals were collected. 16 features were extracted from each breathing signal, and those features were described in the Subsection 2.4.1. Extraction of features was done on MATLAB R2019a software environment.

Features that have higher correlation coefficients than 0.7 for each breathing type were extracted from the feature set. Features were eliminated one by one, checking the correlation after every elimination to keep the maximum number of uncorrelated features. Elimination according to the correlation has been performed on both normalized and not normalized data.

Linear discriminant analysis was performed after the elimination according to the correlation to be able to eliminate non-linearly correlated features, as well. The procedures that are followed to compute the new 4 dimensional feature set is can be found in Appendix A.

Finally, extracted and selected features were fed to the MATLAB's classification learner tool to see the classification algorithm results.

4. RESULTS

This section explains the extraction of the displacement information from the raw data and then compares the results of the measured displacement information with a linear actuator and a respiratory belt. Thereafter, Subject 5's breathing patterns are illustrated and features that are extracted from them are given in a table for each subject. Lastly, classification algorithm results are then given Section 4.6.

4.1 Preliminary Doppler Radar Measurement Setup Results

The designed Doppler radar is illustrated in the Figure 4.1. The hardware dimensions were 56.5 mm for the width and 85.6 mm for the length and lastly the height was 80 mm.

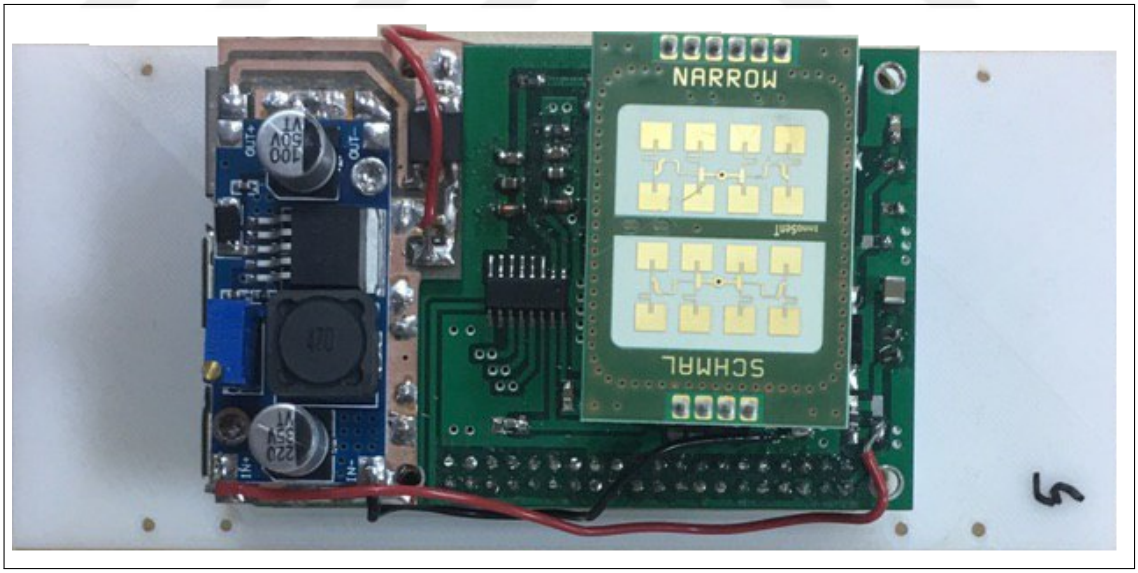

Figure 4.1 Designed Doppler radar measurement system.

Normal breathing respiration movement, cough and apnea mimic from a subject while he was wearing respiratory belt transducer and Doppler radar measurement was focus on the same area results are shown in Figure 4.2.

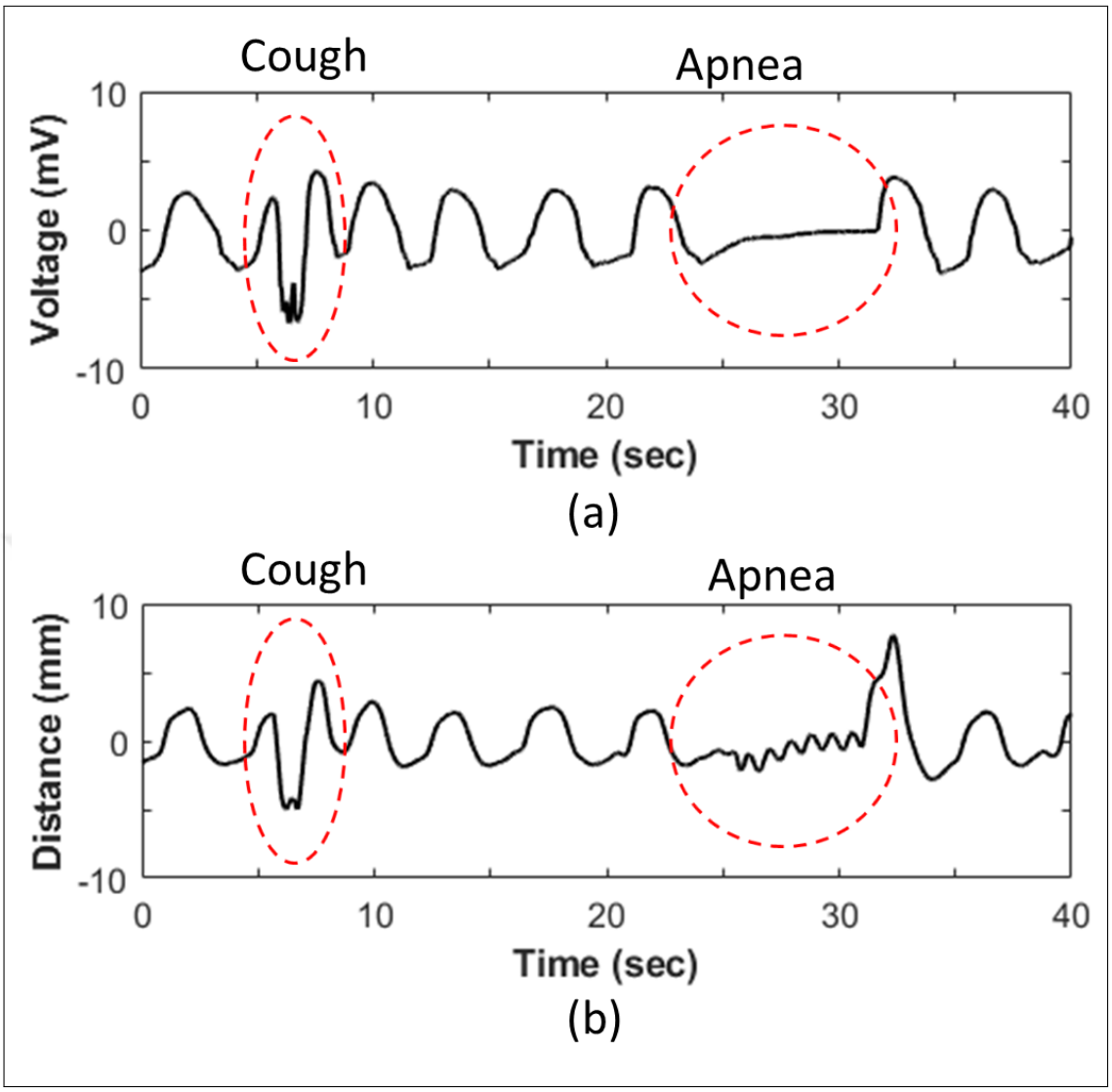

Figure 4.2 Designed Doppler radar measurement system and respiratory belt comparison.

The top graph is taken from the respiratory belt transducer and Y axis represents the voltage that is generated from the transducer of the respiratory belt which caused from the chest wall motion. Second graph at the bottom is the results from designed Doppler radar and Y axis of it shows the chest wall displacement in mm. First red circle on the left side of the plot between 5-8 seconds illustrates the cough mimic of the subject and the second red circle on the right side of the between 24-33 seconds shows the apnea mimic of the subject.

4.2 Linear Actuator Measurement Results

Figure 4.3 shows the course of calculation of distance starting from the collected voltage values. Figure 4.3(a) shows the in-phase (blue) and quadrature (red) channel measurement results for 30 seconds. The amplitude of the channels was scaled to -1 to 1. Figure 4.3(b) is the result of the arctangent demodulation. The result of arctangent demodulation is in between $-\pi$ to $+\pi$ and the unwrapped plot is shown in Figure 4.3(c). In Figure 4.3(d) the black line illustrates the results taken from the controller of the linear actuator. The red line on the same plot is the calculated displacement of linear actuator measured by Doppler radar in millimeters.

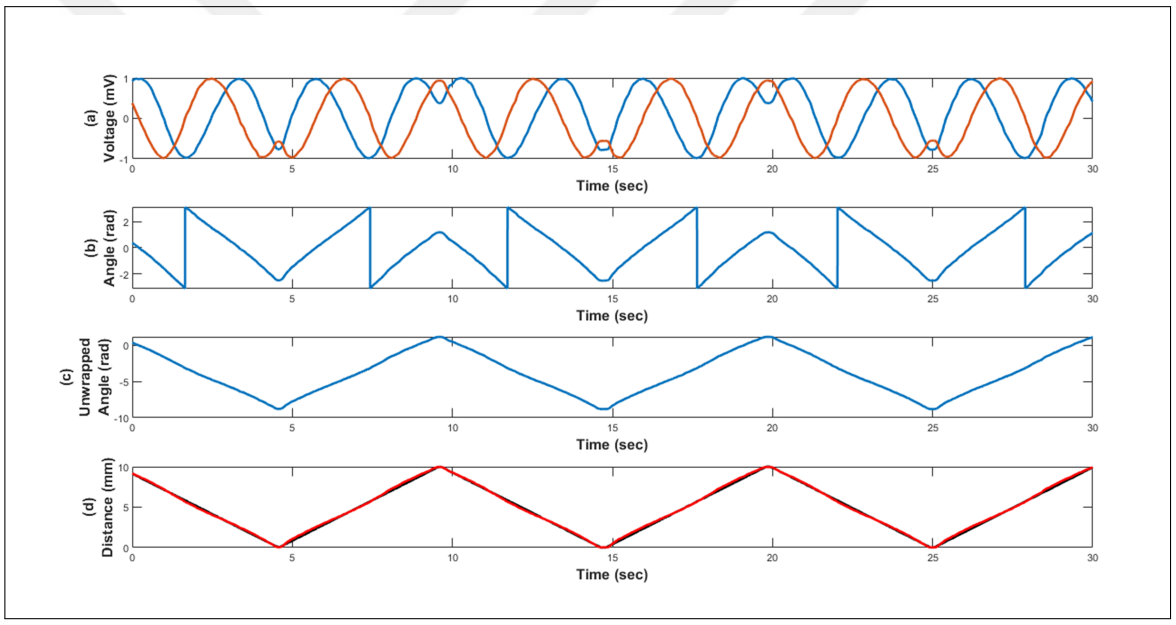

Figure 4.3 Doppler radar displacement extraction steps.

Position information from the linear actuator and Doppler radar displacement measurements given above were compared with Bland-Altman analysis and results were depicted in Figure 4.4. X axis shows the mean of the two different method's position measurements. Y axis shows the difference between all position measurements where the interpolated linear actuator position information was subtracted from the Doppler radar measurements. The black line shows the mean value of the difference in measurements and it is at 0.0594 mm. Red lines are the 1.96 standard deviations added

and subtracted from the mean difference value which are 0.2833 mm and -0.1645 mm respectively. Most of the overrun data are observed when the mean of measurements was between 4mm to 6 mm, but 96.87% of the points were inside the red lines.

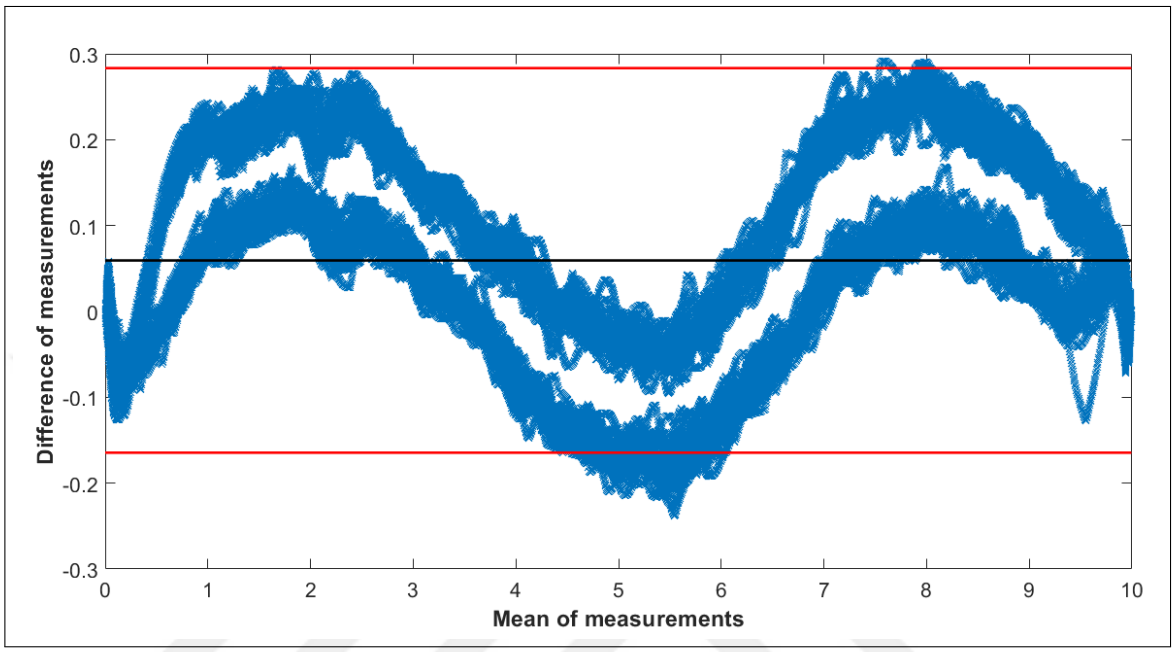

Figure 4.4 Bland-Altman analysis result of Doppler radar vs Linear Actuator.

4.3 Respiratory Belt vs Doppler Radar Measurement Results

Doppler radar and Biopac respiratory effort transducer -MP30 measurement results were shown in Figure 4.5. Subject's chest wall displacement was measured with the Doppler radar, and resulting respiration motion were shown in Figure 4.5(a). Y axis of the graph shows the chest wall displacement in millimeters and maximum displacement is measured to be 11.05 mm. Figure 4.5(b) shows the results from the Biopac respiratory effort transducer -MP30. X axis of both graphs illustrate the time, and measurements were taken for 70 seconds. Y axis for respiratory belt transducer was acquired in voltages. Peak counting indicates that the respiratory rates are equal for both methods. Subject's breath hold (apnea) reproduction takes place between 16-28 seconds for Doppler radar system and for respiratory belt it was seen between 17-28 seconds. While the Doppler radar has shown constant like distance measurements

during the apnea, respiratory belt transducer showed a descending trend.

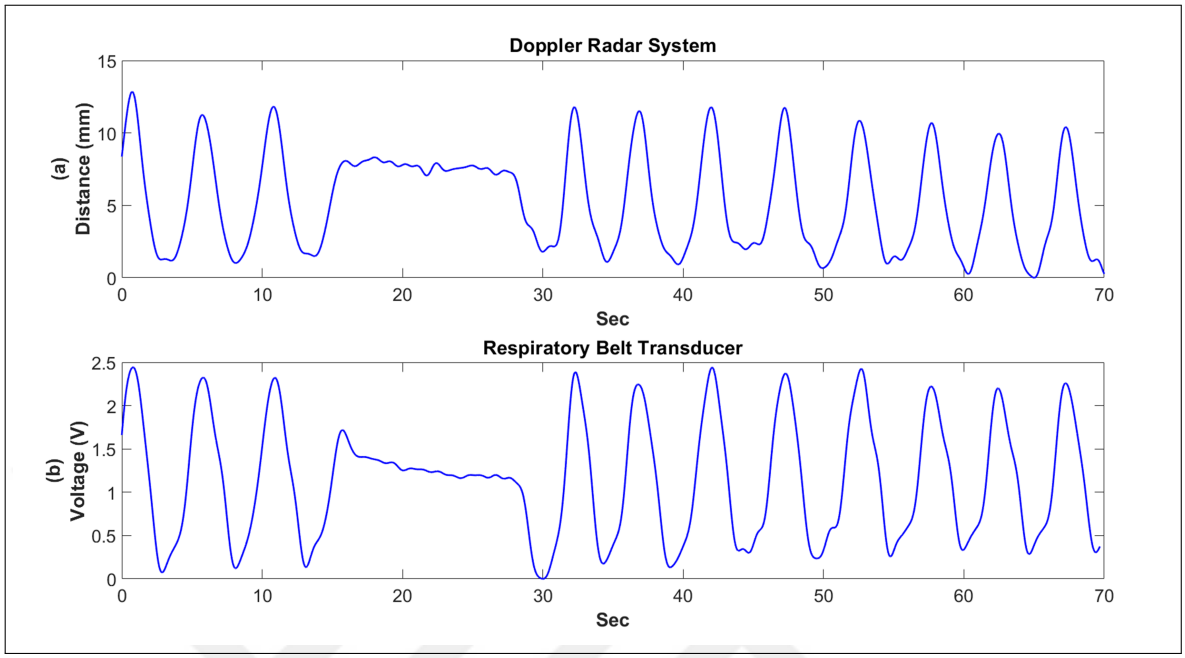

Figure 4.5 Single subject's normal breathing and apnea measurement results of Doppler Radar and Biopac respiratory effort transducer -MP30. Figure 4.5(a) Doppler radar measurement result. Figure 4.5(b) Biopac respiratory effort transducer -MP30 measurement result.

4.4 Breathing Measurement Results

Breathing patterns described in Section 2.1 were reproduced by 10 subjects, resulting chest wall displacement graphs collected from Subject 5 can be seen in Figure 4.6. All breathing patterns were recorded for 60 seconds. Figure 4.6(a)-(e) shows the Biot's, Cheyne-Stokes, hypoventilation, Kussmaul and normal breathing patterns, respectively. During the Biot's breathing measurements, subject 1,3 and 7 took deep breaths and held it which altered the several feature results including maximum peak location, peak average, and peak variability. Moreover, as can be seen in subject 5's breathing result, measurement base-line oscillates during the measurements and this oscillation was seen for all subjects.

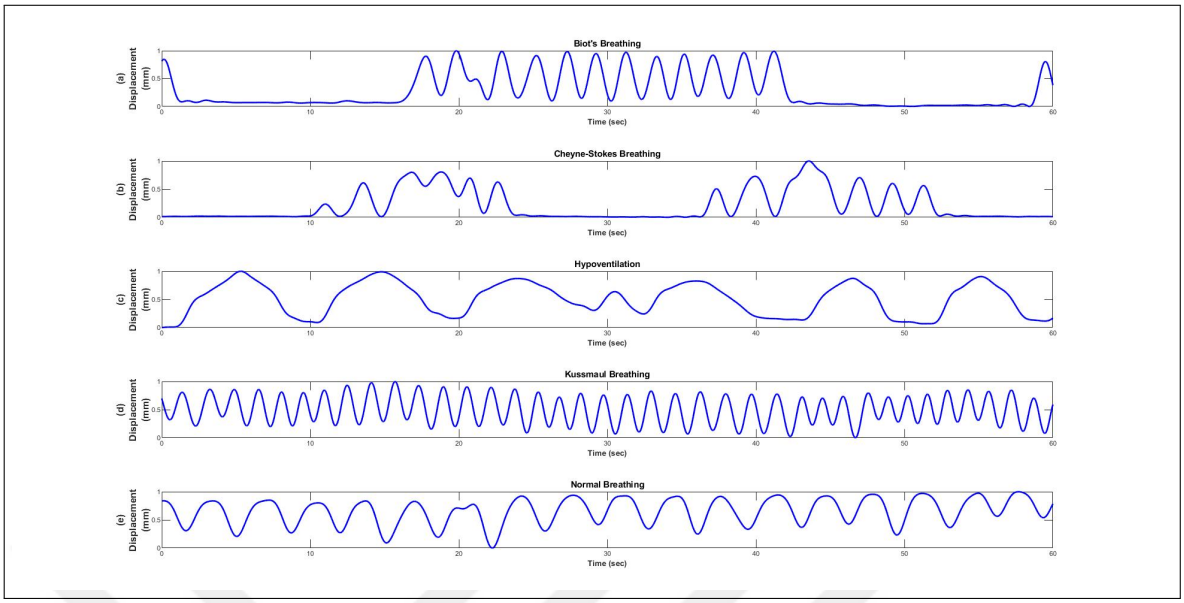

Figure 4.6 Chest wall displacement measurements collected from Subject 5.

4.5 Feature Extraction Results

Table 4.1 shows the results of the extracted features of different breathing patterns collected from Subject 5.

4.6 Classification Algorithm Results

Extracted features were used by several classification algorithms and the ensemble subspace discriminant classifier and linear discriminant classifier resulted the best accuracy by predicting 96% of the data correctly. Figure 4.7 shows the confusion matrix of the linear discriminant classifier results.

	Subject 5's Feature Results	Biot's Breathing	Cheyne-Stokes Breathing	Hypo-ventilation	Kussmaul Breathing	Normal Breathing
60 Seconds Rectangle Window	Entropy	0.015	0.011	0.007	0.044	0.02
	Kurtosis	3.3776	3.7931	3.1342	1.5556	2.0407
	Apnea Score	16295	15824	5927	2742	5008
	Peak Max	7.0864	10.6639	5.0087	10.6856	12.2383
	Peak Count	13	12	6	38	17
	Peak variance	0.1455	3.9631	0.1224	0.5985	0.6472
	Peak average	6.6762	7.0078	4.5631	8.7697	11.0333
5 Seconds Sliding Window	Variability	0.0308	0.0222	0.0306	0.0038	0.0112
	Range	0.4607	0.4613	0.6800	0.2581	0.4675
	Max	0.4609	0.4613	0.7195	0.4650	0.7280
	Min	0.0002	0	0.0395	0.2069	0.2605
Instant Frequency Features	Variability	0.1102	0.0975	0.0075	0.6111	0.1735
	Range	1.5993	1.7049	0.4784	2.5765	1.7782
	Min	-0.700	-1.059	-0.825	-0.935	-0.748
	Max	0.8215	0.8042	0.2464	1.2767	0.8003
	Mean	-0.010	0.004	-0.010	-0.004	0.009

Table 4.1
Mean Subject 5's feature extraction results for each breathing pattern.

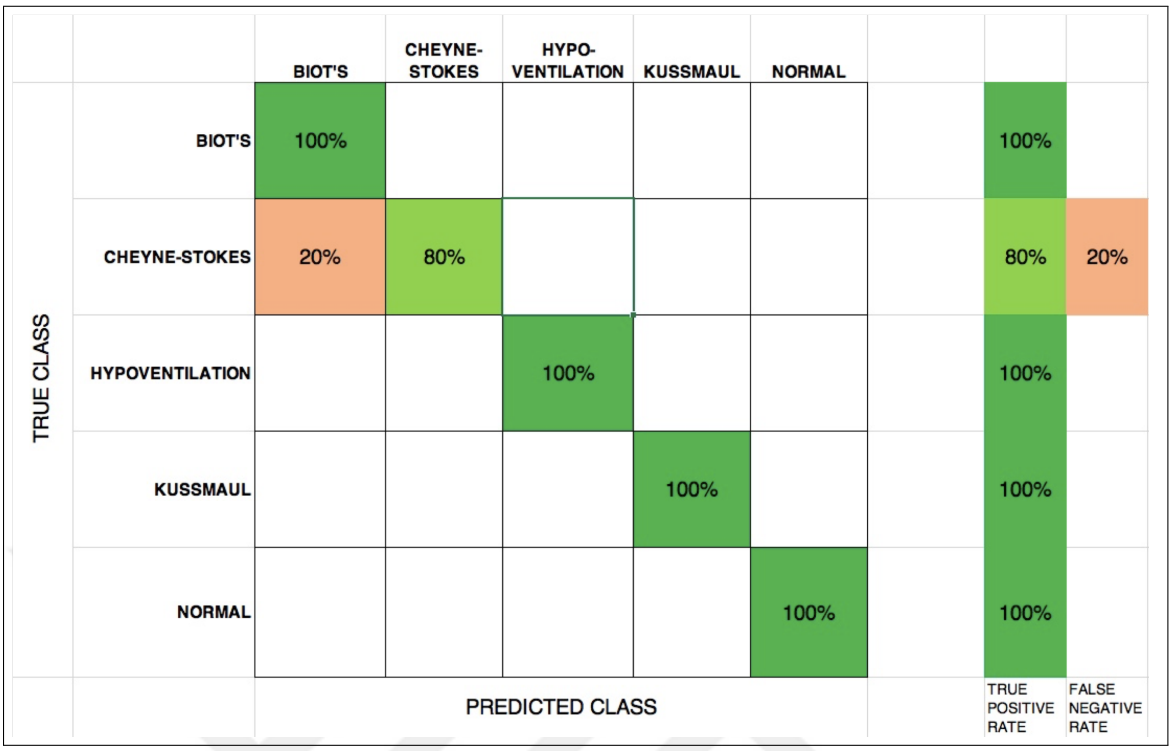

Figure 4.7 Confusion matrix of the linear discriminant classification algorithm.

Table 4.2 shows the different type of classification algorithm results with 10-fold cross-validation when the features were not been normalized. The best-resulted classification algorithms were the linear discriminant (96%) and ensemble subspace discriminant (96%). While linear discriminant falsely predicted 2 Cheyne-Stokes breathing patterns, ensemble subspace discriminant wrongly predicted 1 for Biot's and 1 for Cheyne-Stokes. All the classifiers were predicted the hypoventilation, Kussmaul breathing with 100% precision. Only the linear SVM made 1 false prediction on normal breathing. Cheyne-Stokes was the hardest to predict for the classifiers and weighted KNN has the lowest precision with 70%.

	Accuracy (%)					
Classifier/Breath	Biot's	Cheyne-Stokes	Hypo-ventilation	Kussmaul	Normal	Average
Linear SVM	80	80	100	100	90	90
Subspace Discrt. Ensemble	90	90	100	100	100	96
Fine Decision Tree	90	80	100	100	100	94
Weighted KNN	100	70	100	100	100	92
Linear Discriminant	100	80	100	100	100	96
Gaussian Naive Bayes'	90	80	100	100	100	94

Table 4.2
Classifier algorithm precision results in percentage without normalization of the features.

5. DISCUSSION

Noninvasive and contactless assessment of human physiological condition is desirable for both caregivers and patients. Deterioration of breathing pattern can give an idea about the neurological impairment as mentioned in [1] which makes the contactless monitoring of the breathing pattern desirable. In this thesis, an ARM-based microcomputer device is developed to detect the respiration and heart rate. Although the device is able to detect these vital signs and normal breathing pattern accurately, we were not able to monitor the Cheyne-Stokes and Biot's breathing patterns. The device was also in agreement with respiratory belt transducer during the cough and apnea measurements. Thereby, to be able to detect all breathing patterns described in Section 2.1 IPS -154 Doppler radar module used with the setup described in the Section 3.2. Raw quadrature signals acquired from the Doppler module were filtered with analog components with a 10 Hz cutoff frequency for the anti-aliasing purposes before digitization. To minimize the power supply noise, Rohde Schwarz JMP4030 programmable power supply and LT3042 ultra low noise RF linear regulator was used. Also during the test with the linear actuator, it was observed that grounding the power cables separately decreased the electrical noise on the system significantly.

Quadrature channels were sampled synchronously since any delay in sampling between channels causes phase shifts and this shift affects the arctangent demodulation. As it was recommended in [2], the selected sampling frequency was 500 Hz so that it will be higher than 100 Hz to decrease the out-of-band interference. Sampled signals contain the DC offset stemming from both the internal reflections of RF front-end and from the background object reflections. The respiration frequency of a hypoventilation patient may turn out to be 0.1 Hz, which makes DC offset an issue. One of the ways that was used to get rid of DC offset was AC coupling, which latens the time response of the system drastically. To have a faster time response and computational simplicity, DC cancellation was applied simply by removing the mean from both of the channels, digitally. Mean extracted and scaled raw signals were shown in Figure 4.3(a).

Due to the single channel's null point limitation, arctangent demodulation was used to find the motion of the thorax expansion as it was recommended in the literature [31]. Distance information was found after the signals were arctangent demodulated, converted from radians to angle, unwrapped and converted to distance in millimeters respectively which is shown in Figure 4.3(b-d). Since the distance information contains the heart motion and other unwanted higher than respiration frequency components, a Kaiser window FIR filter with 0.7 Hz cutoff and order of 6272 was used. The solution to using a high order filter was to take 3 minutes of breathing measurements from each subject for each breathing pattern and then extracting the 60 second intervals from it by hand. FIR filter was chosen because of its linear phase which is crucial in our study since we are extracting the distance from the phases of two channels. The signal needed to be truncated by hand as a consequence of the high ordered filter altering the first part of the distance measurement result.

Bland-Altman method is the gold standard statistical analysis to compare two different measurement system which measures the same measurand [38]. The linear actuator system and Doppler radar measurement results are illustrated in Figure 4.3(d). To be able to statistically analyze the Doppler radar and linear actuator measurements the sampling frequency should be the same. As the sampling frequency of the linear actuator is lower (100 Hz) than the Doppler radar's sampling frequency (500 Hz), linear interpolation was performed to the linear actuator. Although other interpolation types could also be selected, in our test setup linear actuator's speed was set to be the same during the measurement so linear interpolation was expected to give better results than the other types. The results of the Bland-Altman analysis was shown in Figure 4.4 and 96.87% of the data were found to be in between the red lines which indicates 1.96 standard deviations added and subtracted from the mean difference value. This implicates that these two measurement setups measure the same thing with similar accuracy. Furthermore, maximum measurement difference result between the linear actuator and the Doppler radar system is 0.53 mm which is very small compared to the distances we want to measure which are generally in the range of 4-12 mm [2].

To investigate the accuracy of the Doppler radar measuring real breathing move-

ments, the system and the respiratory belt transducer monitored the same subject synchronously as in [22, 39] and the Figure 4.5 was obtained as a result. Since the respiratory belt results are in voltage and Doppler system is in millimeters, Bland-Altman analysis could not be used. Figure 4.5 shows the 70 seconds of breathing measurement results while the subject performed normal and apnea. For both methods, the respiration rate is found to be the same as it was expected but the apnea period was found slightly different. This difference is thought to be caused by respiratory belt transducer's high pass filter. Any time the subjects breath in and hold their breath, voltage decrements were seen with descending intervals as it is the case in capacitor discharge.

As a next step, 5 breathing patterns described in the Section 2.1 were collected from 10 subjects. Breathing patterns of subject 5 is plotted in Figure 4.6. For the Biot's breathing pattern, (as it can also be seen in subject 5's results) most of the subjects hold their breath after a deep inhalation which altered many of the features. Features like approximate entropy, maximum peak value, mean, standard deviation and range of the peaks may mislead by this action and affected the results. Biot's breathing classification accuracy was the lowest for every classification algorithm and this may be one of the causes. Cheyne-Stokes breathing was the hardest to perform for the subjects and so the variation within this pattern was found to be higher than other breathing patterns. As mentioned in the Subsection 2.1.3, tidal volume of hypoventilation should be less than normal breathing and results from the subjects show good correlation with this information which can be considered as a good feature to separate these two patterns. To replicate the Kussmaul breathing, subjects were asked breath deep and rapidly which made them dizzy at the end of the procedure. Some of the subjects, as it is the case with subject 5, were not able to breathe with a steady initial chest wall displacement which means the subject did not exhale fully and started a new inhalation. As a consequence, the Kussmaul breathing pattern resulted in a higher variation than it was expected. These fluctuations were also seen in other respiration patterns but with much less amplitude.

Machine learning algorithms performances are strongly dependent on the ex-

tracted features they are fed and that is why extracting and selecting the most definitive features are important. Since a signal can be expressed with an amplitude, a frequency and phase information, features were extracted by considering these properties. Some features such as mean, standard deviation, variability of the peaks are expected to have the good characteristics of amplitude of the signals. To represent the frequency and the phase of the signal, number of peaks, variance, mean, maximum and minimum of instantaneous frequency were extracted. These features were have already been effectively used in the literature [16, 34, 40]. Apnea between two breathing is a discriminative feature so a hand-written apnea detection feature was also used. The result of this feature was as expected and able to discriminate the Biot's and Cheyne-Stokes breathing pattern from the normal breathing, hyperventilation and hypoventilation patterns. Approximate entropy is also a widely used feature to measure the regularity and the periodicity of a time-series data [41, 42]. If we assume the normal breathing to be a perfect sinusoidal signal with constant frequency and amplitude, only the change in frequency affects the approximate entropy and this was also seen in our results as hypoventilation (lower frequency) had the lowest average approximate entropy and Kussmaul breathing (higher frequency) had the maximum average approximate entropy. Kurtosis is another feature used in time-series data and it was a good discriminator for hypoventilation from other breathing patterns in my thesis [43, 44].

A good feature is strongly correlated with the result but not with other features. For a linearly correlated feature set, looking at the correlation of each feature and eliminating the ones with higher correlation coefficients increase the accuracy of the classification algorithm and decreases the required computational power and time. Hence, correlation coefficients of features with one another were calculated, and the features that are highly correlated with other features for all subjects and breathing types were excluded from further evaluations. Peak average of 60 seconds measurement and instant frequency range was found to be correlating with more than 2 features in each breathing so that they were excluded from measurements.

Linear discriminant analysis is another filtering method for feature selection and

it reduces the number of features to a desired number of nxd-dimensional subspace. It works well with linear and nonlinear data sets [37, 45] and it drastically increased the detection of Biot's breathing pattern in my thesis work. Although, features which are not scaled, mislead the distance-based classification algorithms by their variances and magnitudes LDA overcome this problem inherently.

Classification algorithms resulted in good accuracy ranges from 90% to 96%. Cheyne-Stokes breathing was the hardest pattern for the subject it resulted in the subjects breathing patterns. Even when we plot the graphs, variations were clear between subject results but still, the ensemble subspace discriminant was able to classify this breathing pattern with 90% accuracy. Biot's breathing accuracy was always higher than Cheyne-Stokes and when it was misclassified, algorithms predicted it as Cheyne-Stokes breathing. It may be due to the apnea segment for both patterns. All the Kussmaul and hypoventilation predictions were correct for every classification algorithms even though there were deviations in Kussmaul breathing patterns.

Since the normal breathing chest wall displacement is higher than hypoventilation chest wall displacement for the same patient, continuous monitoring is required to predict accurately. Furthermore, with the increased knowledge about physiology and continuous measurements of it, our predictions can be used as assistive information in other diagnoses.

6. CONCLUSION

This thesis aimed to detect breathing disorders remotely using Doppler radar and machine learning algorithms. Chest wall motions were captured using a 24 GHz ISM band Doppler radar. Analog and digital signal processing techniques were used to extract the displacement information from the raw data collected from the Doppler radar. According to the Bland-Altman statistical method the designed radar system was found to be able to accurately detect chest wall displacement. Considering the previous works in the literature and investigation of the signal trends, features were extracted from breathing signals. To increase the speed of computation and exclude the features that represent the same characteristics of the signal, feature selection was applied and the most informative features were fed to the classification algorithms. It was found that the subspace discriminant ensemble and linear discriminant classifier was able to predict the breathing patterns with 96% accuracy.

In the future, we plan to improve our device to be able to detect breathing disorders continuously. The programming language is MATLAB currently but other softwares such as python or C++ can be used and will be implemented as a future work. Also, we plan to measure the real patient chest wall motions and improve our device accordingly. Even though the used programming software was MATLAB in this thesis work, other programming languages python and C++ can accurately result as MATLAB software. Especially the python libraries are wide and reachable for the both feature extraction section and classification part of the thesis. To be able to use the device in hospitals, required clinical tests will done in the future.

APPENDIX A.

Feature extraction and LDA MATLAB Script

```
clear all
clc
close all
files = dir;
files(1:2)=[];
dirFlags = [files.isdir] ;
subFolders = files(dirFlags) ;
CovMat{1}='';
mat = dir('*.mat');
mcount=0;
TDSpeakvar=[];
TDSpeakmax=[];
TDSmin=[];
TDSpower=[];
STDvar=[];
STDrange=[];
STDmax=[];
STDmin=[];
storepks=[];
storelocs=[];
shorttimewindow=5;
menergy=[];
for i=1:length(subFolders)
fprintf('Sub folder #%d = %s\n', i, subFolders(i).name);
cd(subFolders(i).name)
mat = dir('*.mat');
figure('Name',subFolders(i).name)
```

```
for q = 1:length(mat)
    s=load(mat(q).name);
CovMat = [CovMat struct2cell(s)];
CovMat{1,q+1+mcount}(:,1)=CovMat{1,q+1+mcount}(:,1)-...
CovMat{1,q+1+mcount}(1,1);
CovMat{1,q+1+mcount}(:,2)=CovMat{1,q+1+mcount}(:,2)-...
min(CovMat{1,q+1+mcount}(:,2));
DetectApnea(:,q+mcount)=length(find(diff(TDSignals)...
<= (0.2*std(diff(TDSignals))) &  diff(TDSignals)...
>= (0.2*-std(diff(TDSignals)))));
storesignals{:,q+mcount} =TDSignals/max(TDSignals);
myangle(:,q+mcount)=(TDSignals*2*pi*24e9)/(1000*3e8);
cen_ang(:,q+mcount) = myangle(:,q+mcount)-mean(myangle(:,q+mcount));
inst_fre(:,q+mcount) = diff(cen_ang(:,q+mcount))/(1/500)/(2*pi);
ifa(:,q+mcount)=medfilt1(inst_fre(:,q+mcount),60);
kurtosisResults(:,q+mcount) = mean(ifa(:,q+mcount).^4)...
/(mean(ifa(:,q+mcount).^2)).^2;
t=CovMat{1,q+1+mcount}(:,1);
t2=find(t>=0 & t<=shorttimewindow ); % SHORT TIME x axis
        N=length(t2);
nTDSignals=TDSignals/max(TDSignals);
for j=1:size(nTDSignals,1)-size(t2,1)
menergy(j,q)=sum(nTDSignals(j:size(t2,1)+j-1,1).^2)...
 /(size(t2,1));
end
TDSmin=[TDSmin min(TDSignals)];
TDSpower=[TDSpower  sum(TDSignals.^2)/size(TDSignals,1)];
STDvar=[STDvar sum( abs( menergy(:,q)-mean(menergy(:,q))).^2 )...
/(size(TDSignals,1)- size(t2,1)-1)];
STDmax=[STDmax max(menergy(:,q))];
STDmin=[STDmin min(menergy(:,q))];
STDrange=[STDrange STDmax(end)-STDmin(end)];
```

```
subplot(length(mat),1,q);
findpeaks(TDSignals,t,'MinPeakProminence',2,'MinPeakDistance',0.75)
[pks,locs] =findpeaks(TDSignals,t,'MinPeakProminence',2,...
'MinPeakDistance',0.75);
storepks{1,q+mcount}=pks;
storelocs{1,q+mcount}=locs;
TDSpeakcount(q+mcount)=length(pks);
TDSpeakavr(q+mcount)=mean(pks);
TDSpeakvar(q+mcount)=var(pks);
TDSpeakmax(q+mcount)=max(pks);
mangle(:,q+mcount)= 2*pi*24e9*TDSignals/(1000*3e8);
cen_ang(:,q+mcount) = mangle(:,q+mcount)-mean(mangle(:,q+mcount));
inst_fre(:,q+mcount) = diff(cen_ang(:,q+mcount))/(1/500)/(2*pi);
insmax(q+mcount)=max(inst_fre(:,q+mcount));
insmin(q+mcount)=min(inst_fre(:,q+mcount));
insvar(q+mcount)=var(inst_fre(:,q+mcount));
insmean(q+mcount)=mean(inst_fre(:,q+mcount));
insrange(q+mcount)=insmax(q+mcount)-insmin(q+mcount);
approxEnt(q+mcount) = approximateEntropy(TDSignals,'Radius',
0.1*std(TDSignals),'Dimension',2);
    end
    mcount=mcount+length(mat);

end

%%% Class names
mnames=["Biots" "Biots" "Biots" "Biots" "Biots" "Biots" "Biots"
"Biots" "Biots" "Biots" "CheyneStokes" "CheyneStokes"
"CheyneStokes" "CheyneStokes" "CheyneStokes" "CheyneStokes"
"CheyneStokes" "CheyneStokes" "CheyneStokes" "CheyneStokes"
"Hypoventilation" "Hypoventilation" "Hypoventilation"
"Hypoventilation" "Hypoventilation" "Hypoventilation"
```

```
"Hypoventilation" "Hypoventilation" "Hypoventilation"
"Hypoventilation" "Kussmaul" "Kussmaul" "Kussmaul" "Kussmaul"
"Kussmaul" "Kussmaul" "Kussmaul" "Kussmaul" "Kussmaul"
"Kussmaul" "Normal" "Normal" "Normal" "Normal" "Normal"
"Normal" "Normal" "Normal" "Normal" "Normal" ];
sefa=table(TDSpeakavr',TDSpeakvar',TDSpeakmax',TDSpeakcount'
,STDmin', STDmax',STDrange',STDvar',insmax',insmin',insrange'
,insvar',insmean', approxEnt',kurtosisResults',DetectApnea'
,mnames');
CovMat(1)=[];
mydata=[TDSpeakvar',TDSpeakmax',TDSpeakcount',STDmin',STDmax'
,STDrange', STDvar',insmax',insmin',insvar',insmean'
,approxEnt',kurtosisResults',
DetectApnea'];

X=mydata;
mdims=4;
[classes, bar, labels] = unique(mnames);
classnum = length(classes);
CSw = zeros(size(X, 2), size(X, 2));
CSt = cov(X);
for i=1:classnum
    % Instances
    instX = X(labels == i,:);
% Within class scatter
CovMat = cov(instX);
p = size(instX, 1) / (length(labels) - 1);
CSw = CSw + (p * CovMat);
end
% Between class scatter
BCS = CSt - CSw;
BCS(isnan(BCS)) = 0; CSw(isnan(CSw)) = 0;
```

```
BCS(isinf(BCS)) = 0; CSw(isinf(CSw)) = 0;
% Check dimensions
if classnum <= mdims
mdims = classnum - 1;
warning(['Target dimensionality reduced to ' num2str(mdims) '.']);
end
% Perform eigendecomposition of inv(Sw)*Sb
[M, lambda] = eig(BCS, CSw);
% Sort eigenvalues and eigenvectors in descending order
lambda(isnan(lambda)) = 0;
[lambda, ind] = sort(diag(lambda), 'descend');
M = M(:,ind(1:min([mdims size(M, 2)])));
% Mappdata
mappedData = X * M;
% Store mapping for the out-of-sample extension
mapping.M = M;
mapping.val = lambda;
LdaReducedMatrix=mydata*mapping.M;
MLfeatures=table(LdaReducedMatrix(:,1),LdaReducedMatrix(:,2),...
LdaReducedMatrix(:,3),LdaReducedMatrix(:,4),mnames');
```

REFERENCES

1. Jerome B. Posner M.D., Clifford B. Saper M.D., Nicholas Schiff M.D., F. P. M., *Plum and Posner's Diagnosis of Stupor and Coma*, Contemporary Neurology Series, Oxford University Press, 2007.

2. Boric-Lubecke, O., V. M. Lubecke, A. D. Droitcour, B. K. Park, and A. Singh, *Doppler Radar Physiological Sensing*, Wiley, 2016.

3. Silbernagl, S., and A. Despopoulos, *Color Atlas of Physiology*, stuttgart: Thieme, 6th ed., 2009.

4. Dougherty, L., and S. Lister, "Clinical Nursing Procedures," 2015.

5. European Respiratory Society, S., *Respiratory Diseases in the World. Realities of Today âĂŞ Opportunities for Tomorrow*, European Respiratory Society, 2013.

6. Yuan, G., N. Drost, and A. McIvor, "Respiratory Rate and Breathing Pattern," *McMaster University Medical Journa*, Vol. 10, no. 1, pp. 23–25, 2013.

7. Dennis, Mark and Talbot Bowen, William and Cho, L., *Mechanisms of Clinical Signs 2nd Edition*, Vol. 61, Elsevier, 2nd revise ed., 2015.

8. Golby, A., D. McGuire, and L. Bayne, "Unexpected recovery from anoxic-ischemic coma," *Neurology*, Vol. 45, pp. 1629 LP – 1630, aug 1995.

9. Wijdicks, E. F. M., J. E. Parisi, and F. W. Sharbrough, "Prognostic value of myoclonus status in comatose survivors of cardiac arrest," *Annals of Neurology*, Vol. 35, no. 2, pp. 239–243, 1994.

10. Wijdicks, E. F. M., "Biot's breathing," *Journal of Neurology, Neurosurgery and Psychiatry*, Vol. 78, no. 5, pp. 512–513, 2007.

11. Mimoz, O., T. Benard, A. Gaucher, D. Frasca, and B. Debaene, "Accuracy of respiratory rate monitoring using a non-invasive acoustic method after general anaesthesia," *British Journal of Anaesthesia*, Vol. 108, no. 5, pp. 872–875, 2012.

12. Zhang, Z., J. Zheng, H. Wu, W. Wang, B. Wang, and H. Liu, "Development of a respiratory inductive plethysmography module supporting multiple sensors for wearable systems," *Sensors (Switzerland)*, Vol. 12, no. 10, pp. 13167–13184, 2012.

13. Mazzanti, B., C. Lamberti, and J. de Bie, "Validation of an ECG-derived respiration monitoring method," in *Computers in Cardiology, 2003*, pp. 613–616, IEEE, 2003.

14. Al-Khalidi, F. Q., R. Saatchi, D. Burke, H. Elphick, and S. Tan, "Respiration rate monitoring methods: A review," *Pediatric Pulmonology*, Vol. 46, no. 6, pp. 523–529, 2011.

15. Fekr, A. R., M. Janidarmian, K. Radecka, and Z. Z. Radecka, "A medical cloud-based platform for respiration rate measurement and hierarchical classification of breath disorders," *Sensors (Switzerland)*, Vol. 14, no. 6, pp. 11204–11224, 2014.

16. Fekr, A. R., M. Janidarmian, K. Radecka, and Z. Zilic, "Respiration Disorders Classification With Informative Features for m-Health Applications," *IEEE Journal of Biomedical and Health Informatics*, Vol. 20, pp. 733–747, may 2016.

17. Lohman, B., O. Boric-Lubecke, V. M. Lubecke, P. W. Ong, and M. M. Sondhi, "A digital signal processor for Doppler radar sensing of vital signs," in *Annual Reports of the Research Reactor Institute, Kyoto University*, Vol. 4, pp. 3359–3362, 2001.

18. Rabbani, M. S., and H. Ghafouri-Shiraz, "Accurate remote vital sign monitoring with 10ÂăGHz ultra-wide patch antenna array," *AEU - International Journal of Electronics and Communications*, Vol. 77, pp. 36–42, 2017.

19. Suzuki, S., T. Matsui, M. Kagawa, T. Asao, and K. Kotani, "An approach to a non-contact vital sign monitoring using dual-frequency microwave radars for elderly care," *Journal of Biomedical Science and Engineering*, Vol. 06, no. 07, pp. 704–711, 2013.

20. Miao, D., H. Zhao, H. Hong, X. Zhu, and C. Li, "Doppler radar-based human breathing patterns classification using Support Vector Machine," *2017 IEEE Radar Conference, RadarConf 2017*, pp. 0456–0459, 2017.

21. Rahman, Tauhidur, Adams, A. T., R. V. Ravichandran, M. Zhang, S. N. Patel, J. A. Kientz, and T. Choudhury, "DoppleSleep: A contactless unobtrusive sleep sensing system using short-range Doppler radar," *UbiComp*, pp. 39–50, 2015.

22. Lee, Y. S., P. N. Pathirana, C. L. Steinfort, and T. Caelli, "Monitoring and Analysis of Respiratory Patterns Using Microwave Doppler Radar," *IEEE Journal of Translational Engineering in Health and Medicine*, Vol. 2, no. March, 2014.

23. Rahman, A., V. Lubecke, E. Yavari, X. Gao, and O. Boric-Lubecke, "High dynamic range DC coupled CW Doppler radar for accurate respiration characterization and identification," *89th ARFTG Microwave Measurement Conference: Advanced Technologies for Communications, ARFTG 2017*, Vol. 4, no. 1, pp. 1–4, 2017.

24. Skolnik, M., *Radar Handbook*, McGraw-Hill Education, third edit ed., 2008.

25. Tworzydlo, P., *Monitoring Breathing Using a Doppler Radar*. Master's thesis, Carleton University, 2016.

26. Naceur, A., and A. Khalfa, "Analysis Study of Radar Probability of Detection for Fluctuating and Non-fluctuating Targets," *Algerian journal of signals and systms (AJSS)*, Vol. vol. 2, pp. 12–20, 2017.

27. Toomay, J. C., *Radar Principles for the Non-Specialist*, Dordrecht: Springer Netherlands, 1989.

28. Byung-Kwon Park, S. Yamada, O. Boric-Lubecke, and V. Lubecke, "Single-channel receiver limitations in doppler radar measurements of periodic motion," *2006 IEEE Radio and Wireless Symposium*, pp. 99–102, 2006.

29. Droitcour, A. D., S. Member, O. Boric-lubecke, S. Member, V. M. Lubecke, S. Member, J. Lin, S. Member, G. T. A. Kovacs, and A. D.-c. Doppler-radar, "Range Correlation and I = Q Performance Benefits in Single-Chip Silicon Doppler Radars for Noncontact Cardiopulmonary Monitoring," *IEEE Transactions on Microwave Theory and Techniques*, Vol. 52, no. 3, pp. 838–848, 2004.

30. Shinozuka N, Y. Y., "Measurement of fetal movements using multichannel ultrasound pulsed Doppler: autorecognition of fetal movements by maximum entropy method.," *Medical & Biological Engineering & Computing.*, Vol. 31(1), no. July, pp. S59–Z66, 1993.

31. Park, B. K., O. Boric-Lubecke, and V. M. Lubecke, "Arctangent demodulation with DC offset compensation in quadrature Doppler radar receiver systems," *IEEE Transactions on Microwave Theory and Techniques*, Vol. 55, no. 5, pp. 1073–1078, 2007.

32. Alpaydin, E., *Introduction to Machine Learning*, MIT Press, 2010.

33. Pincus, S. M., "Approximate entropy as a measure of system complexity.," *Proceedings of the National Academy of Sciences of the United States of America*, Vol. 88, pp. 2297–2301, mar 1991.

34. Chon, K., C. Scully, and S. Lu, "Approximate entropy for all signals," *IEEE Engineering in Medicine and Biology Magazine*, Vol. 28, no. 6, pp. 18–23, 2009.

35. Alex Smola, S. V., *Introduction to Machine Learning*, Cambridge University Press, 2008.

36. Quinlan, J. R., "Induction of Decision Trees," *Machine Learning*, 1986.

37. Li, T., S. Zhu, and M. Ogihara, "Using discriminant analysis for multi-class classification: An experimental investigation," *Knowledge and Information Systems*, Vol. 10, no. 4, pp. 453–472, 2006.

38. Glantz, S. A., and S. Glantz, *Primer of Biostatistics: Sixth Edition*, Lange Medical Books, McGraw-Hill Companies,Incorporated, 2005.

39. Sun, G., and T. Matsui, "Rapid and stable measurement of respiratory rate from Doppler radar signals using time domain autocorrelation model," *Proceedings of the Annual International Conference of the IEEE Engineering in Medicine and Biology Society, EMBS*, Vol. 2015-Novem, no. 3, pp. 5985–5988, 2015.

40. Qiu, L., and G. Li, "Representation of ECG signals based on the instantaneous frequency estimation," *International Conference on Signal Processing Proceedings, ICSP*, Vol. 2, pp. 1731–1734, 1996.

41. Holzinger, A., C. Stocker, M. Bruschi, A. Auinger, H. Silva, H. Gamboa, and A. Fred, "On applying approximate entropy to ECG signals for knowledge discovery on the example of big sensor data," *Lecture Notes in Computer Science (including subseries Lecture Notes in Artificial Intelligence and Lecture Notes in Bioinformatics)*, Vol. 7669 LNCS, pp. 646–657, 2012.

42. Guo, S., Y. Hu, J. Guo, and W. Zhang, "An EMG-based muscle force evaluation method using approximate entropy," *2016 IEEE International Conference on Mechatronics and Automation, IEEE ICMA 2016*, pp. 1197–1202, 2016.

43. Shen, C. L., T. H. Huang, P. C. Hsu, Y. C. Ko, F. L. Chen, W. C. Wang, T. Kao, and C. T. Chan, "Respiratory Rate Estimation by Using ECG, Impedance, and Motion Sensing in Smart Clothing," *Journal of Medical and Biological Engineering*, Vol. 37, no. 6, pp. 826–842, 2017.

44. Dubey, H., N. Constant, and K. Mankodiya, "RESPIRE: A Spectral Kurtosis-Based Method to Extract Respiration Rate from Wearable PPG Signals," *Proceedings - 2017 IEEE 2nd International Conference on Connected Health: Applications, Systems and Engineering Technologies, CHASE 2017*, no. June, pp. 84–89, 2017.

45. Duda, R. O., P. E. Hart, and D. G. Stork, *Pattern Classification*, Wiley Interscience, 2000.